ABSTRACT

Title of Thesis: INFLATABLE ACOUSTIC METAMATERIAL

Haafiz Husker
Master of Science, 2021

Thesis Directed by: Professor Amr Baz
Department of Mechanical Engineering

Acoustic metamaterials thus far have been either passive or employed stacking to produce wide range of results. With the advent of advanced additive manufacturing techniques, the ability to create novel metamaterials have increased. Usually these Acoustic Meta Material are passive like in case of Membrane-type and Plate-type metamaterials. They are usually thin membranes or plates consisting of periodic unit cells with added masses. Numerous studies have shown these metamaterials exhibit tunable anti resonances with transmission loss greater than their corresponding mass-law. In these studies, the tunability usually results in complex electrical architecture and furthermore, in most of the investigations it is assumed that the unit cell edges of the metamaterial are fixed.

In this study, an innovative method is explored to create an active metamaterial that can be easily tuned. The proposed method distinguishes itself from past contributions by employs a unique unit cell design that is fabricated via advanced additive manufacturing to create a metamaterial that exhibits negative Poison's

ratio with adjustable unit cell edges for greater transmission loss than its mass-law would otherwise suggest. The membrane like Metamaterial is tuned by inflating itself with pressurized air. The pressurization leads to large non-linear deformation and geometric stiffing in the membrane apart from adding mass by expanding its elastic unit cell edges. Which is exploited to adjust the eigen-modes and sound loss of the structure.

The veracity of this proposed design is then investigated analytically and experimentally. The metamaterial is manufactured using elastic material called Agilus-30 via Multi-jet Manufacturing and is tested in an impedance tube to see its trans- mission loss. Finite elemental analysis is done to reduce the computational effortin creating an analytical model. The finite element analysis is compared with the experimental results to arrive at a consensus. The proposed metamaterial is then tested in real life application by conducting frequency response on a headphone with the IAMM installed to truly understand, the performance of such a setup. The results of these tests indicate the range of performance across low and high frequency as well as the versatility of the metamaterial to be adapted into any size as per the requirement.

INFLATABLE ACOUSTIC METAMATERIAL

by

Haafiz Kallupurackal Husker

Thesis submitted to the Faculty of the Graduate School of the
University of Maryland, College Park in partial fulfillment
of the requirements for the degree of
Master of Science
2021

Advisory Committee:
Prof. Amr Baz, Chair/Advisor
Prof. Balakumar Balachandran
Prof. Hosam Fathy

Dedication

I dedicate my thesis to my parents and grandparents. For fostering my passion and giving me their undying support, hard work and love.

Acknowledgments

I owe my gratitude to all the people who have made this thesis possible and because of whom my graduate experience has been one that I will cherish forever.

First and foremost, I would like to thank my advisor, Dr. Amr Baz for giving me an invaluable opportunity to work on challenging and extremely interesting projects over the past three years. It has been a pleasure to work with and learn from such an extraordinary individual with such great knowledge in this field of Vibroacoustics.

My colleagues at the Smart Materials and Structure Research Center (SMSRC) have enriched my graduate life in many ways and deserve a special mention. I would also like to acknowledge help and support from the staff members at Terrapin Works for greatly enabling me the freedom to tinker with multiple designs.

Thanks to Dr. Fathy and Dr. Balachandran for sparing their invaluable time reviewing my manuscript and agreeing to be on my committee It is impossible to remember all, and I apologize to those I've inadvertently left out.

Lastly, thank you all and thank God!

Table of Contents

List of Tables

List of Figures

List of Abbreviations

AAM	Active Acoustic Metamaterial
ABS	Acrylonitrile Butadiene Styrene
AM	Additive Manufacturing
ASTM	American Society of Testing and Materials
CAD	Computer Aided Design
dB	Decibel
DC	Direct Current
IAMM	Inflatable Acoustic Metamaterial
FEA	Finite Elemental Analysis
FEM	Finite Element Modelling
FFF	Fused Filament Fabrication
FFT	Forward Fourier Transform
MJM	Multi Jet Manufacturing
MAM	Membrane-type Acoustic Metamaterial
PLA	Poly Lactic Acid
PMAM	Perforated Membrane-type Metamaterial
SLA	StereoLithography Apparatus
SPL	Sound Pressure Level
STL	Sound Transmission Loss
TL	Transmission Loss
UV	Ultraviolet

Chapter 1: Introduction

1.1 Introduction to Metamaterial

Metamaterial is a nascent field in material science that has piqued the interest of scientists due to their various applications. Metamaterials are engineered to have properties or behaviors that are usually not found in conventionally occurring materials. They are fashioned out of assemblies that are usually arranged in repeating patterns at a scale smaller than the wavelength of the phenomena they influence. The term metamaterial was initially coined in the late 1990s for composite materials that were specifically designed to yield unusual electromagnetic properties [1]. Their precise structure, shape, geometry, orientation and arrangement gives them the peculiar properties that can manipulate electromagnetic waves by blocking, absorbing, enhancing or even bending them, which are not easily possible with conventional materials.

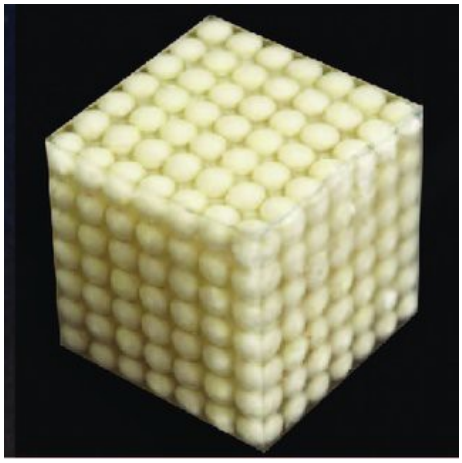

Figure 1.1: Metamaterial with locally resonant wave propagation. [2]

Metamaterial can be fundamentally defined as artificially crafted materials that derive their properties from their internal structure rather than their own material properties. These repeated units can be described as the 'atoms' of the metamaterial and hence by manipulating the shape, structure and lattice of these structural units, obtain different properties can be obtained from these metamaterials. This in no way means there are no naturally occurring metamaterials, one main example being Zeolites.

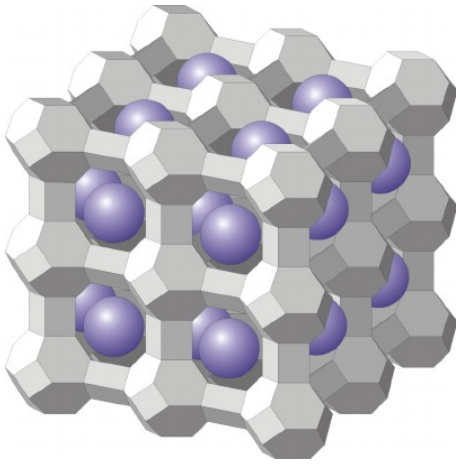

Figure 1.2: Example for naturally occurring metamaterial: Zeolites withpeculiar lattice structure. [3]

Metamaterials, on a fundamental level, can be described as a plethora of systems that are engineered to exhibit certain properties. These metamaterials are instrumental in altering or managing wave behaviors and hence are usually used in those fields that tend to involve them. Metamaterials were first borne out of ways to manage light waves by their differential refractive indices. They then have been further used in electric and magnetic wave theories.

The term "*metamaterial*" was coined for specifically designed composite material that yield unusual physical properties like negative permittivity and permeability [1]. In regard to electromagnetism, such extraordinary materials were first investigated by Pendry *et al* [4, 5], even though it was Smith *et al* [6] who provided experimental evidence of materials producing negative permittivity and permeability. These, along with the works of Veselago *et al* [7] and Shelby *et al* [8], paved the way for applications of metamaterials in electromagnetism. Due to their common characteristics like wave propagation, metamaterials were implemented into other wave behaviors like light and sound.

1.2 Metamaterials in Acoustics

The first venture into acoustic metamaterial is widely considered to be the investigation of locally resonant sonic crystals by Liu *et al* [2], that had periodically arranged sub wavelength sized spheres coated with elastic materials. They exhibited high transmission loss and low frequency band caused by their effective density. In the years that followed, various other types of acoustic metamaterials were investigated. These studies were pertaining negative density [9-

12], bulk mod- ulus [13-14] and double negative properties [15-17]. Such special properties helped create applications ranging from diodes [18], cloaks [19] to acoustic super lenses [21].

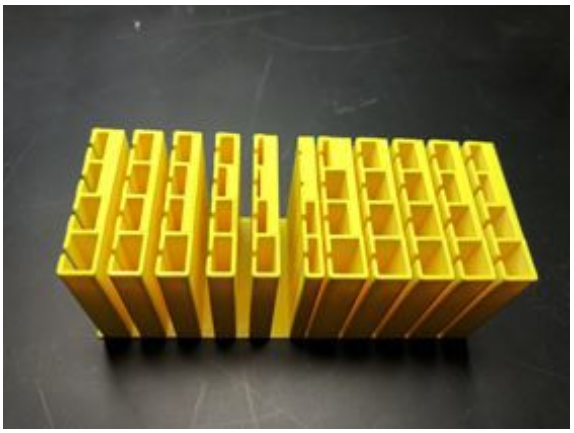

Figure 1.3: **Example 3D printed material using multi-volumes Helmholtz resonators to control sound wave propagation By Duke University**

Inflatable Acoustic Metamaterial is inherently a membrane-type metamaterial (*MAM*) as the name suggests. The first iteration of such metamaterial is alluded in the study by Yang and colleagues [10], which explored negative dynamic mass of such metamaterials. These were instrumental in fields that require lightweight structures and deal with small space for utilization, such as field of aerospace. Essentially, these *MAMs* were composed of pre-stressed, thin, membrane-like walls withattached masses that enable static tuning. These 2-D structures at low frequencies could exhibit transmission loss several orders lower than its corresponding mass-law dictates [10, 22].

These MAMs faced a certain drawback; that once manufactured, these meta-materials could not be tuned. They were found to be inept in applications where there was a shift in tonal parts or even change in pre-stress in the membrane due

to outside factors like temperature, wear and tear were to be considered. Various methods like stacking pre-configured MAMs with different frequency to create a panel were explored [22]. This panel enabled transmission loss at multiple frequencies and allowed for the shifting tonal components. Such pre-configured MAMs caused the weight and space required for the installation to be higher, therebylosing the novelty and edge these metamaterials possessed.

1.3 Active Acoustic Metamaterials

A considerable radical approach to overcome this narrow band characteristics was to shift from passive metamaterial to an active one. Dr. Baz was the first to investigate active acoustic metamaterial (AAMs) [22-23] and with W. Akl [24-25], he implemented piezoelectric materials to tune the effective density and bulk modulus of the sound treatment. This concept of programmable bulk modulus led to the creation of an active acoustic diode that could adjust effective properties over a large range [26]. Others have tried to amalgamate AAMs with MAMs to form Active Membrane type Metamaterial. The initial attempt was to incorporate magnetorheological membrane into the MAM which was then controlled by an external magnet. These membranes are smart fluids that change its property, mainly viscosity, when subjected to magnetic fields, this enabled the control of the pre-stress in the membrane via the external gradient magnetic field, which in turn allowed to shift eigenfrequency of the membrane. The major drawback of the proposed idea by Chen *et al.* [27] was the weight and size as the external magnet drastically increase both spaces for installation as well as the weight.

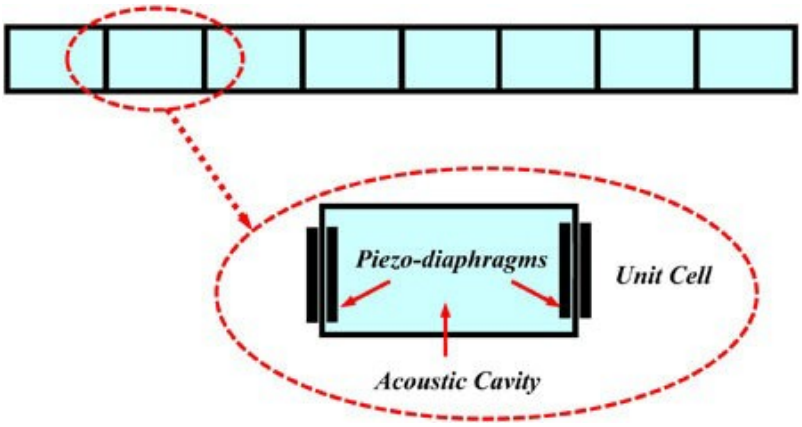

Figure 1.4: Active acoustic metamaterial by Dr. Baz, with piezo diaphragms on either side of the cavity to produce negative effective density

Similarly, F. Langfeldt and colleagues from Hamburg University of Applied Science (HAW, Hamburg) realized an *AMAM* that employs an impeller that is more centralized for manipulating dynamic metamaterial properties without sacrificing the main attraction of such metamaterials, *i.e.*, light weight and the space involved [28]. A novel method of pressurized air was used for the actuation of the *AMAM*cell that altered the pre-stress of the membrane itself. It involved two vertically stacked *MAM* that were framed airtight in order to have a fixed air volume between them that could later be used to expand. Air volume between these membranes could be pressurized with static differential pressure using simple external source of pressurized air via tubing inside [28]. The advantage of this kind of actuation for manipulating the acoustic properties was the ease of availability of such mechanisms.Since pressurized air is more readily available in passenger transport vehicles with air conditioning and even trains and aircrafts, this increases the application of such *AMAMs*. The differential pressure inside the airtight membrane

couple, leads to non-linear geometric deflection and increases the stiffness in the membranes [28]. This led to the increasing of the eigen-frequencies and thus an opportunity to exploitand tune the metamaterial.

1.4 Concept Behind Inflatable Acoustic Metamaterial

1.4.1 Acoustic Background

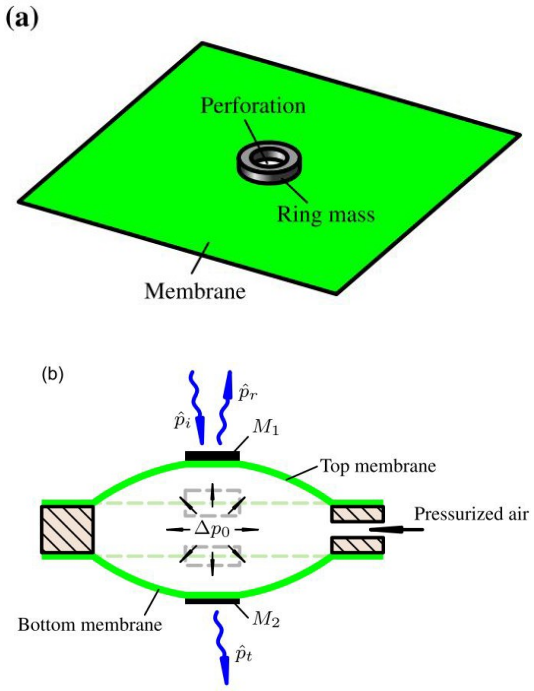

Figure 1.5: Membrane with perforation for added mass and the cross section view of the AMAM unit cell by Dr Langefeldt [28]

In acoustic metamaterials, the transmission loss can be described through the mass-law. The mass-law is a relationship between surface mass density and transmission loss.

$$TL = 20log_{10}\frac{\omega\sigma}{2Z_0} \tag{1.1}$$

Where $\omega = 2\pi f$ is the angular frequency, σ is the supposed surface mass density of the material and the Z_0 is the characteristic impedance. As aforementioned, mostly membrane type acoustic metamaterials (*MAM*s) possess low frequency bands that have high transmission loss. In order to achieve broadband noise insulation, two main ways usually explored were stacking multiple *MAM* unit cells and adding mass to each cell, thereby taking advantage of the mass law. As discussed, this usually leads to redundancy as adding more mass increases weight. In the study following the inflated *MAM* cell, F. Langfeldt *et al* [29] researched the advantage of perforated membrane like acoustic metamaterial (*PMAM*s). The idea was to use the phenomenon found in Helmholtz resonators to the already fledgling acoustic metamaterial. The perforation acted akin to the neck of the Helmholtz resonator, as the air volume trapped behaved acoustically like added mass, thus taking advantage of mass-law to increase transmission loss.

1.4.2 Design and structural Background

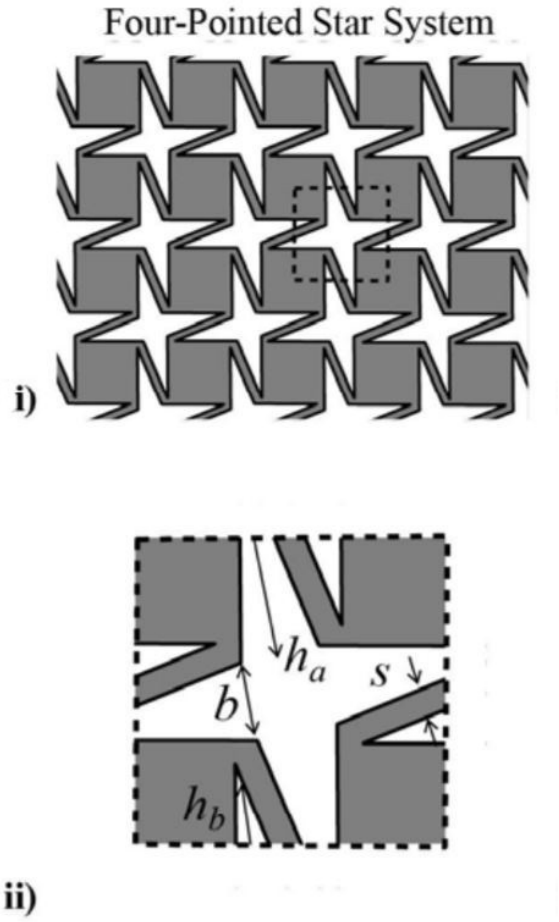

Figure 1.6: Infinite tessellations with the repeating unit for four star perforations proposed by L. Mizzi *et al* [31]

Auxetic materials are special mechanical metamaterials that exhibit negative Poisson's ratio. In the work of Bianchi and Scarpa [30], transmissibility and damping behavior of such unconventional foam materials were found to be better than expected. Thus, their unconventional geometry that imparts negative Poisson's ratio under duress, making such auxetic materials a mechanical metamaterial, also behaves like acoustic metamaterial. L. Mizzi *et al* [31] proposed a new direction to

create such auxetic foams incorporating new manufacturing concepts. Since these metamaterials require unique geometrical shapes to give them their intrinsic characteristic anomalies, novel manufacturing techniques like additive manufacturing provide a new foray like never before. In the study, Mizzi and colleagues studied the auxetic behaviors of new perforated mechanical metamaterials using n-pointed star shaped pores that were manufactured using stereolithography. It was found that on experiencing strain, the reconfigured unit cell showed negative Poisson's ratio.

1.5 Scope of the thesis

The present contribution is an amalgamation of past work done in the field of acoustic metamaterials. The noise attenuation of Inflatable Acoustic Meta-Material (IAMM) with star shaped perforations is explored in the presented work. Advanced additive manufacturing is used to create four-point star shaped perforations with an elastic, proprietary non-linear membrane-like material. The perforation is subjected to strain via inflation and hence, the pre-stress in the membrane is manipulated to create tunability in attenuation. Initially, theoretical analysis be- hind the inflatable acoustic metamaterial (*IAMM*) is investigated concurrently with finite element analysis to understand the ramification of the proposed model with regards to sound transmission loss and eigen-frequencies. Then, advanced additive manufacturing technique is employed to create the prototype which is then tested experimentally inside an impedance tube to verify the analytical model. Further, a real life implication of such a prototype is created

by installing Inflatable Acoustic Metamaterial inside a noise cancelling headset and tested for frequency response using KEMAR manikin to see the performance for noise cancelling.

1.6 Summary

This chapter presented and explained the concept of metamaterials and its application in various fields of wave theory. Many trailblazing works by past researchers have been listed in this chapter that essentially became the cornerstone of this concept. Applications and salient features of various types of acoustic metamaterial is discussed in this chapter. The works that form the prerequisites for the design and the theory behind the Inflatable acoustic metamaterial (*IAMM*) is laid out. In this chapter, the method of validating and consolidating the prototypes performance is explained.

Chapter 2: Manufacturing of Inflatable Acoustic Metamaterial

2.1 Overview

Acoustic metamaterials are said to possess their peculiar properties due to the structure that it encompasses rather than its material properties. Most often, these intricate models are hard to manufacture even with the help of traditional machining. The advent of additive manufacturing (*AM*) has paved new ways that enableus with greater flexibility in shapes that can be produced. There exists different additive manufacturing techniques that can be utilized to produce the structure thatis required. The pros and cons were weighed to determine the optimum method.

Additive manufacturing can be distinguished by the method or material used as filament based (*FFF*), resin based (*SLA*) or inkjet based (*MJM*). Most of these methods build layer by layer, and in the case of resin based stereolithography and MultiJet modelling, point by point aspect is also followed. Each additive technique provides certain advantages and disadvantages.

In case of Fused Filament Fabrication, semi molten thermoplastic like Acrylonitrile Butadiene Styrene (*ABS*) or Poly Lactic Acid (*PLA*) is extruded through a nozzle via roller onto a build plate to produce easily malleable plastic designs that are often inexpensive and favorable for rapid prototyping. These hot filaments solidify

in due time when exposed to room temperature [32]. The drawback with six-axis arm-controlled nozzle is the limited freedom in manufacturing internal structures. Extensive support material are required for complex designs. There is also a matter of material limitations as materials are limited to hard plastic-like products that are brittle or semi flexible. This technique impedes the desired results that are sought in manufacturing *IAMM*, which requires membrane-like flexibility and should be

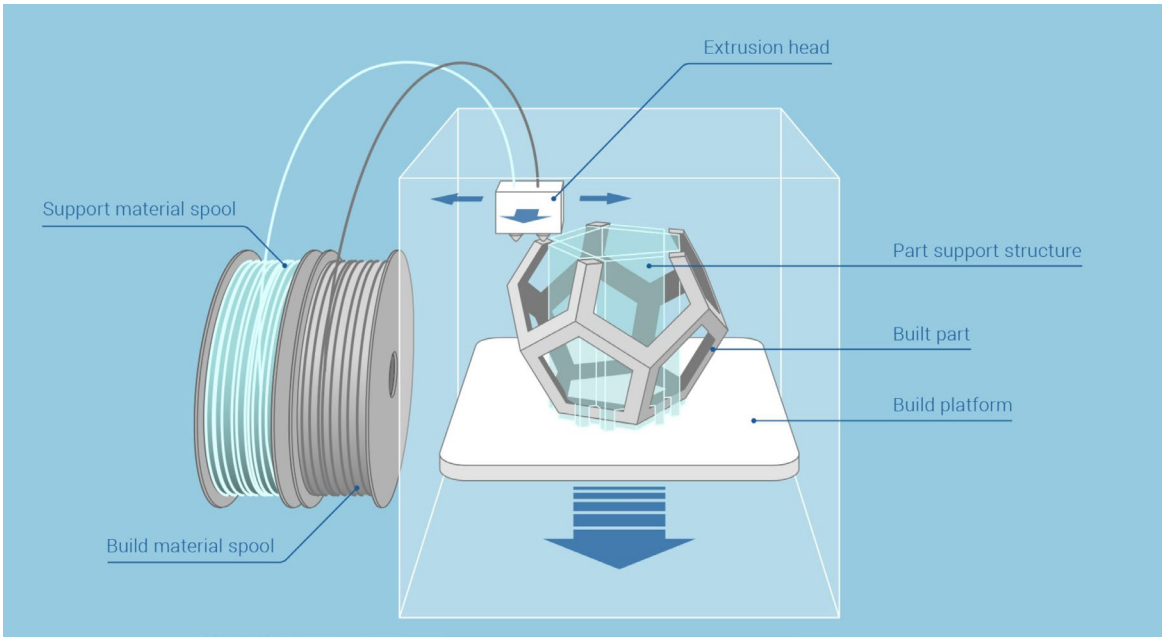

Figure 2.1:Schematic representation of Fused Filament Fabrication

The next progression in additive manufacturing is resin based stereolithography *(SLA)* which provides a wider range of materials and design complexity than fused filament fabrication *(FFF)*. However, it negates the inexpensive nature, speed and ease of manufacturing. It follows a layer by layer, point by point nature wherein it utilizes an ultraviolet *(UV)* beam to cure a layer point by point from a vat of designated material resin [32]. This point-by-point approach coupled with the post-processing of curing and baking the specimen after printing increases the manufacturing time considerably. The extensive post processing is due to the material being a viscous liquid. It also requires support structures to facilitate structures that are interior and intricate in its complexity. This, when involved with elastic material, prevents the kinds of finish and property that are sought for the *IAMM*. When printing with elastic resins, complex interior structures that require support structure while being printed are hard to fabricate as lack of rigidity causes the structure to fail. Rigidity to an extent is essential to make sure that the structuredoes not shear or fail when inflated.

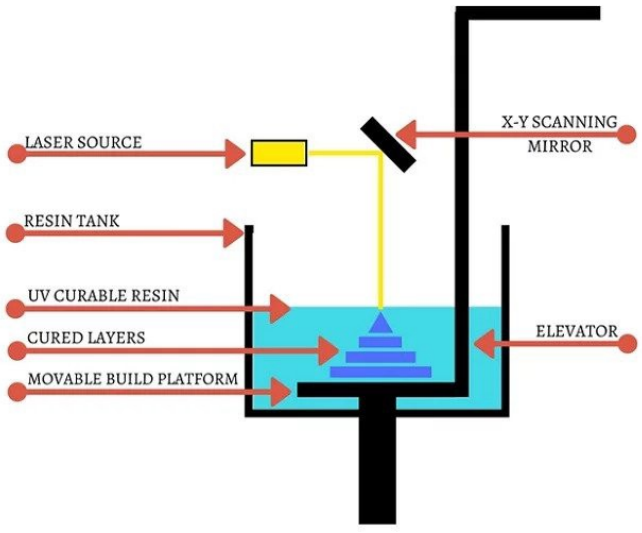

Figure 2.2: Schematic representation of Stereo-lithography

A more advanced additive manufacturing techniques that is available is Ink-jet based MultiJet Modelling (*MJM*), where droplets of ink-like material are dropped layer by layer concurrently with sacrificial support material as required. These ink droplets are photosensitive and are hence cured by using light as compared to ultraviolet in stereo-lithography. The print head drops the material and cures it in one go, thereby reducing considerable amount of post processing compared to *SLA*. Multi-Jet Manufacturing (*MJM*) provides the greatest flexibility in design complexity as it enables the ability to produce intricate designs within the structure as it is being manufactured. The support materials are water soluble and hence can be removed by dissolution or water jet. It also offers a wide range of different materials that have flexible and rigid nature in varying degrees. This is because *MJM* provides the opportunity to mix inks to obtain the right consistency and property required. *MJM* provides the ability to print multiple materials in a single print job, which was not the case in prior techniques. Unlike *FFF* or *SLA*, *MJM* technique is not cost effective as it is the more expensive of the three.

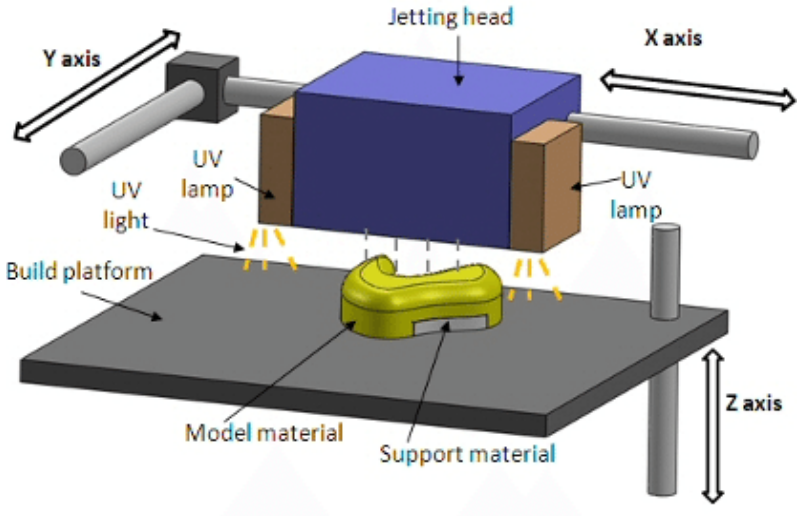

Figure 2.3: Schematic representation of Multi-jet manufacturing.

In this project, it is vital that air tightness is ensured to make sure the evaluation is verified. Even though MJM enables manufacturing the whole apparatus in a single go, due to constraints pertaining to support material removal, time and cost, the prototype is separated into three different parts to cut down on time and efficiency. Hence, post processing time by submerging the apparatus in chemical sonic bath or sonicator to remove the internal support structure is only required for the metamaterial portion.

2.2 Parts of the IAMM

The most integral step is finalizing the apparatus structure that will exhibit negative Poisson's ratio. In the work by Mizzi and colleagues [31], star shaped perforations were found to exhibit negative Poisson's ratio. The aspect of utilizing this phenomenon for noise attenuation is furthered with the help of additive manufacturing. The prototype is separated into three components:

a) Case - the protective shell for the perforated metamaterial structure
b) Flanges - that will be used for coupling the apparatus to the impedance tube
c) The metamaterial, the structure that exhibits noise attenuation properties

Certain components of the IAMM require specific material properties. The lid and bottom are rigid and transparent hence bio-compatible MED610 was used. The case and metamaterial should possess elastic property in order to undergo deformation, Agilus 30 was used to provide them. The flanges and the interlocking projections were required to be rigid and show plasticity therefore Vero-plastic was utilized.

PARAMETER	AGILUS 30	VERO PLASTIC	MED610
Young's Modulus (MPa)	0.5	2600	2500
Density (g/cm^3)	1.125	1.175	1.18
Poison's Ratio	0.4	0.5	0.33

Table 2.1: Material Properties of Raw Material [35-36]

2.3 Case for the metamaterial

The IAMM apparatus is required to be airtight and transparent. These conditions are for accurate transmission loss measurement and the ability to see the expansion of the unit cell in the metamaterial when inflated respectively. Apart from such aesthetic requirements, the material should also be able to withstand the pressure that the metamaterial is subjected to. Thus, taking into consideration of such constraints, the case that holds the metamaterial structure must be robust and secure. Novel sealing techniques were sought in order to achieve the air tightnessas printing the whole prototype as a whole component was counterproductive in terms of post processing. The interlocking mechanism is essentially rigid projectionsthat slot into a elastic pocket to create a colinear joint. The frictional adhesive created between the rubber-like Agilus-30 and Veroplastic rigid material enhances the grip. The edges were filleted to ensure greater finish, and this eradicated any possibility of air leak from the corners that was prevalent in completely 3D printed models. The dimensional constraints for the tube had to be greater than 35mm x 35mm in cross section. The case and sealant are multi-material, the top and bottom are transparent in order to make the deformation visible while the case andlock system

were Agilus-30 and veroplastic respectively.

2.3.1 Pre-processing

The main aim of the case is the provide robustness to the metamaterial whilst making sure the apparatus is airtight. The case is fashioned as a box and lid setup, while frictional contact coupling was utilized to ensure grip. There were multiple design scenarios to be taken into account. the main criteria were robustness to withstand the pressure, clear sight on the internal metamaterial to ensure that it is deformed when actuated and the air tightness. The solution for the robustness was to create the case with the same elastic material as the metamaterial. This is dueto the fact that Agilus-30 shows delayed plasticity when undergone severe stress and hence do not fail. This also ensures that the sound from the impedance tube only interacts with one material thus fortifying the results by making sure no discrepancies are found. In order to provide a clear visual to ensure proper deformation of the perforation inside, the lid is printed with transparent rigid material MED610.

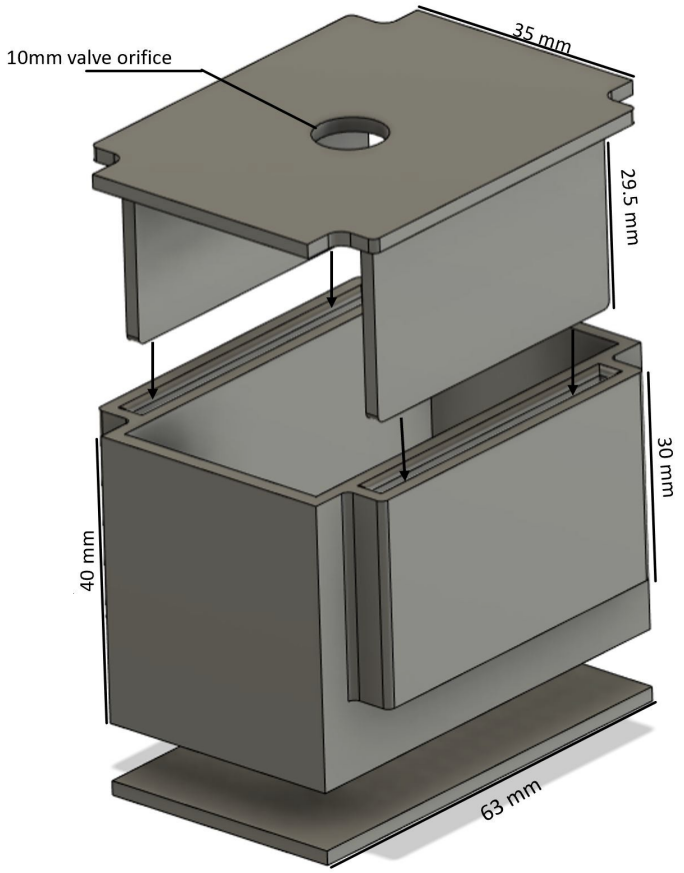

Figure 2.4: Case with the interlocking system and their dimensions.

The integrity of the air seal is maintained by first creating a friction contact bond and then fortifying the seams with hard setting industrial epoxy binders. The lid is provided on either sides with rigid fin like extension that slots into the respective divots made in the case, thus creating an interlocking system. The divots are made with the elastic material while the projections are rigid, this is done in order to take advantage of the grip these interacting surfaces provide when they are created as an interference fit. The interlocking system is not provided across the whole side as they are created 7mm away from the flanges and 6mm away from the bottom. in order to give space for the bolt heads when the *IAMM* is fastened to the

tube.

The case is of the dimensions 63mm x 35mm x 35mm, the 35mm corresponds to the diameter of the impedance tube. This had to be taken into consideration as the case should cover the whole inlet of the impedance tube to give veracity to the results. The lid and the bottom are each of 2mm thickness, this is also reflected in the wall thickness of the case. The thickness provides a membrane like behaviorto the apparatus.

2.4 Flanges for coupling

In the case of impedance tube, there are certain prerequisites for the prototype to be modelled. The prerequisites range from conditions of air tightness to avoid leakage to innovative ways to fasten the perforations to the tube. The dimension of the case is 63x35x25mm, the width and height corresponds to the aforementioned inlet ID of 35mm of the impedance tube

2.4.1 Pre-processing

The flanges are the supporting structure that had to be modelled to fasten the prototype to the impedance tube easily. It is designed as discs on either side of the case with holes of 8-mm holes impinged to match ones on the impedance tube for screws. The flanges possess a 35mm diameter hole for the passage of the sound, which corresponds to the inlet diameter of the impedance tube and hence wouldbe covered by the metamaterial. The screw holes on the flange are spaced out

equidistant by placing them on the vertices of an equilateral inscribed on a circle of radius 28.5 mm respectively. The impedance tube end is circular in nature but on the other hand the metamaterial case has a square cross-section. Therefore, the flange is designed to seamlessly transition into the case with minimal change of area.

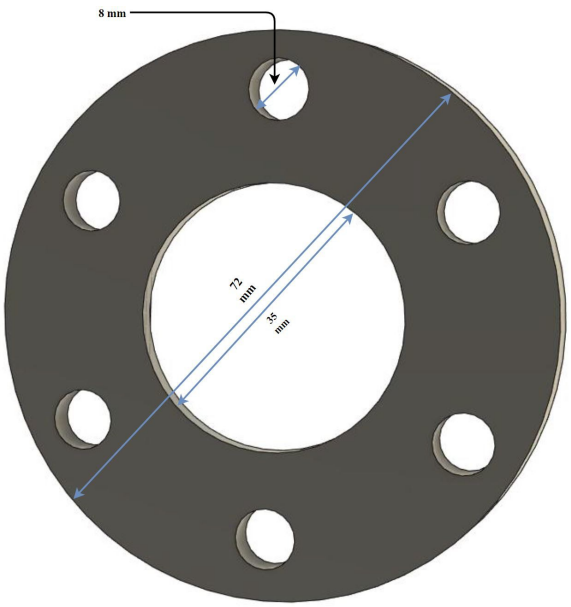

Figure 2.5: Wire-frame representation of the flange with its dimensions.

This change in size and cross-section if present would pose another design obstacle. In order for the passage of sound to be unobstructed and to get an accurate reading, the change in cross section should be avoided. It is very imperative that the 8mm screw hole has sufficient space for the bolts to hold the prototype onto the impedance tube. The change in area of air flow, which has to be taken into account for the numerical analysis due the conical connection between the circular end and square end, is then negated by creating a flush join between the case and the circular base.

2.5 Perforated metamaterial

The interior of the prototype holds the acoustic metamaterial in place. In order to impart the inflatability, it is very imperative that the structure be flexible yet robust enough not to fail. For this versatility, *Poly-jet* printing was chosen for the manufacturing. *Poly-jet* printing provides a wide array of materials with different physical properties ranging from mechanical stiffness to thermal resistance. It also enables lesser manual work as only post processing is required to remove the support material and hence has lesser chance of print failure. Apart from the higher resolution of printing, the support material is also water soluble, thus decreasing the post processing time.

2.5.1 Pre-processing

The pre-processing step in manufacturing the metamaterial consists of the design and modelling. The design for the four-point star configuration is adopted from the work of Mizzi and colleagues [31]. In that work, auxetic behavior of certain peculiar structures were explored. Auxetic materials are those materials that exhibits negative Poisson's ratio. In layman terms, that implies the structures expand when undergoing tensile loading rather than contract. Such materials in the past have been recorded to have shown strong acoustic damping properties. In the aforementioned work by Mizzi and colleagues [31], the star like perforationsin the membrane are constructed with strict dimensional parity with each other.

Essentially, the triangles of the star are to be constructed with

$$h/b = (h^2 + b^2)(0.5)/s \tag{2.1}$$

Where h and b are the height and width of the triangles respectively, while s is the width the link that outlines the perforation. The perforations are made to resemble a tetra-chiral system with square-shaped nodes interconnected by slender ligaments [31].Due to a lack of symmetry, horizontal ligaments would deform more than their vertical counterparts. This non-linearity in deformation causes the structure to exhibit negative Poisson's ratio. Taking advantage of *poly-jet* printing's resolution, the width s was 0.6mm, while height and width were 5mm and 1.5mm respectively. This effectively reduces the unit cell size while maximizing the number of unit cells in the given space. As per the aforementioned study, in order to accelerate the non-linear deformity, the vertical ends are fixed to a 2mm wall. This also acts as a covering that flushes with the flanges thus negating any kind of air leak or counter flow. *Autodesk Fusion 360* was used to create the 3D model of the metamaterial structure. The file was then exported as an "STL" file for printing.

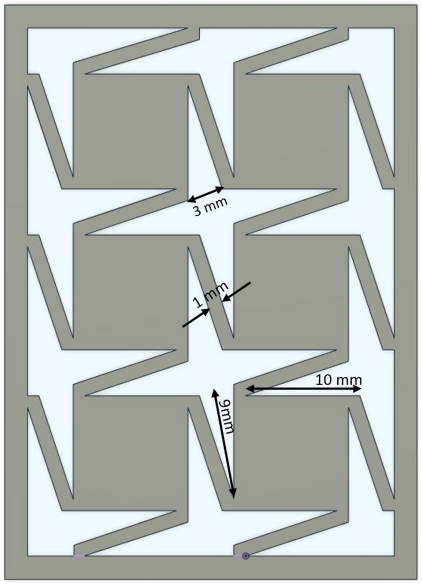

Figure 2.6: Metamaterial structure encompassed by the case with b=3mm, h=9mm and s=1mm

The build plate assembly of the structure was straight forward as there is a genuine lack of constraint. The structure in itself is within the build-plate dimensions and hence was printed on a coordinate system same as the structure. The structure's perforations are filled with support materials.

2.6 Printing and Post-processing

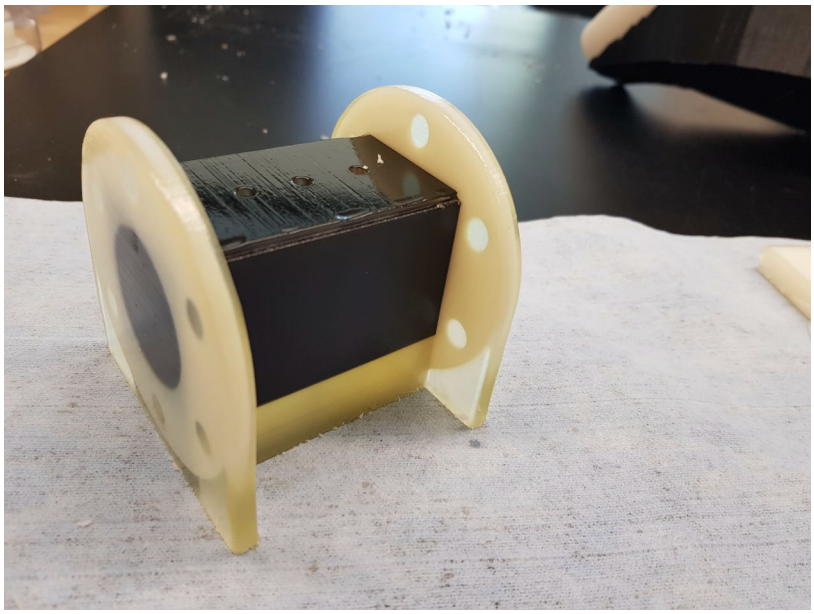

Figure 2.7: Prototype with support material intact

Poly-jet, printing also known as Multi-jet Manufacturing (MJM), is used to create the structure. The need for the structure to inflate and deflate brings the needof the print material to be elastic. *Stratasys Connex3 Objet500* [34] is the printer used to create the metamaterial structure. It essentially uses photopolymers that are deposited according to the model layer by layer and cured using light in one go. The rubber like elastic photo-polymer material used is called Agilus 30. This is a proprietary material by *Stratasys* and provides a wide range of uses. The support material is deposited on the build plate with the material itself and the print-job is manufactured in a suspended matrix of support material. In order to ease the removal from the build plate as well as to reduce any warping or destruction of theprint job while detaching from the build plate, the prototype is made on a bed of support material to uphold the weight. The *Connexx Objet500* [34] uses a gel-like

photopolymer called *Fullcure 705*[34] as the support material. This is essentiallya water-soluble material that can be removed either via chemical bath sonicator or water jet. Since the main structure contains many fragile parts that should not lose its structural integrity, it is very imperative that extreme pressure like the water jet not be used. Hence on account of this, multiple iterations of manual material removal were coupled with bouts in the sonicator to melt away the support materials around the print job.

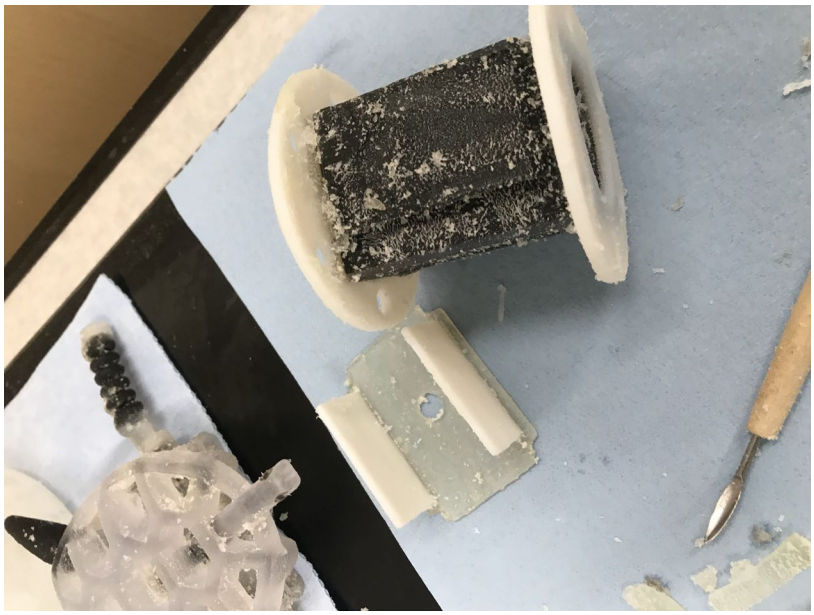

Figure 2.8: Prototype with the support material manually removed

Sonicator is essentially a chemical bath coupled with a vibrator that enables the soluble support material to wiggle off the print job. The print job is usually submerged in a chemical vat solution that contains a mixture of Sodium Metasilicate, Isopropyl alcohol and water. This chemical solution enables faster dissolution

of the non-toxic Fullcure 705 [34]. This, coupled with the sonicator, enables the loose and dissolving support materials to fall out and settle in the chemical solution. Yet, this alone would not be enough to remove all the support structure as the perforation design creates multiple crevices that the solution cannot reach or which the sonicator cannot loosen. Therefore, the sonicator treatment was coupled with manual removal. The crevice was thoroughly cleaned via tools, and bigger support material particles were excavated or broken down before exposing to another round in the sonicator. It is not advised to run the sonicator treatment long because it can cause material degradation. This is something to be avoided as in this case, the structural integrity is paramount to functioning of the prototype. Therefore, the prototype was subjected to sonic bath in 30 min intervals with constant evaluation to makesure the material did not degrade. The material degradation can be of multiple forms, which can range from shedding to warping of the whole structure itself.

Figure 2.9: Prototype is immersed in the chemical solution and is kept in the sonicator

Once the parts are cleaned and support material completely removed, the main structure must be sealed.

2.7 Actuation apparatus

The Inflatable acoustic metamaterial is actuated in both positive and negative controls by using an air pump.The case lid was prepared with a 10mm diameter orifice,which was designated for the valve for the air movement.The whole IAMM apparatus is further sealed using an resin epoxy to ensure critical bonding at the seams. A nipple valve was utilized, the valve was bonded to the orifice with the same epoxy bonding agent.

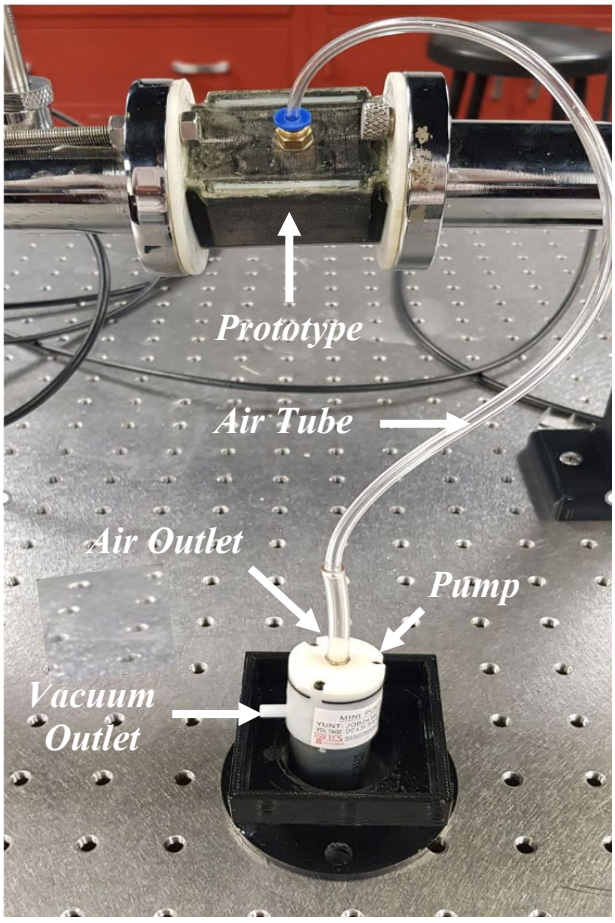

Figure 2.10: Apparatus setup with actuation

A 6-volt DC air pump was used to create the necessary actuation. The air pump has a pressure rating of The pumpis attached using a 4mm diameter clear tube that is interlocked into the valve. Theair pump is capable of producing both vacuum and air, this is creatively used to produce both the required control conditions. In order to maintain the needed pressure/vacuum and to ensure the system is evaluated as a linear time invariant (LTI) system, a pinch valve is attached closer to the valve to shut off any return flow.

2.8 IAMM installed headset

In order to truly assess the performance of IAMM, the prototype is installed in a headset and frequency response tested. The constrains to be kept in mind are that the headset is sealed to ensure that the IAMM is actuated correctly. In order to ensure that the headset would be sealed, a sheet of latex was used. Epoxy resin adhesive was used to seal the latex to the headset. The metamaterial perforation used inside the headset has three star shaped perforations and has dimensions of 45mm x 45mm x 35mm. The prototype foam is fixed in place by foam tape to make sure while actuation the IAMM would not move around. The headset is fastened to the manikin with an earmuff to ensure there isn't leakage of sound.

The actuation of the IAMM is facilitated by the nipple valve just like in case of impedance tube testing. A 6-volt DC air and vacuum pump was utilized to create the necessary pressure inside the headset. The latex sheet ensures the air is kept inside and no air or sound leaks. The ear cushions also aids in this regards.

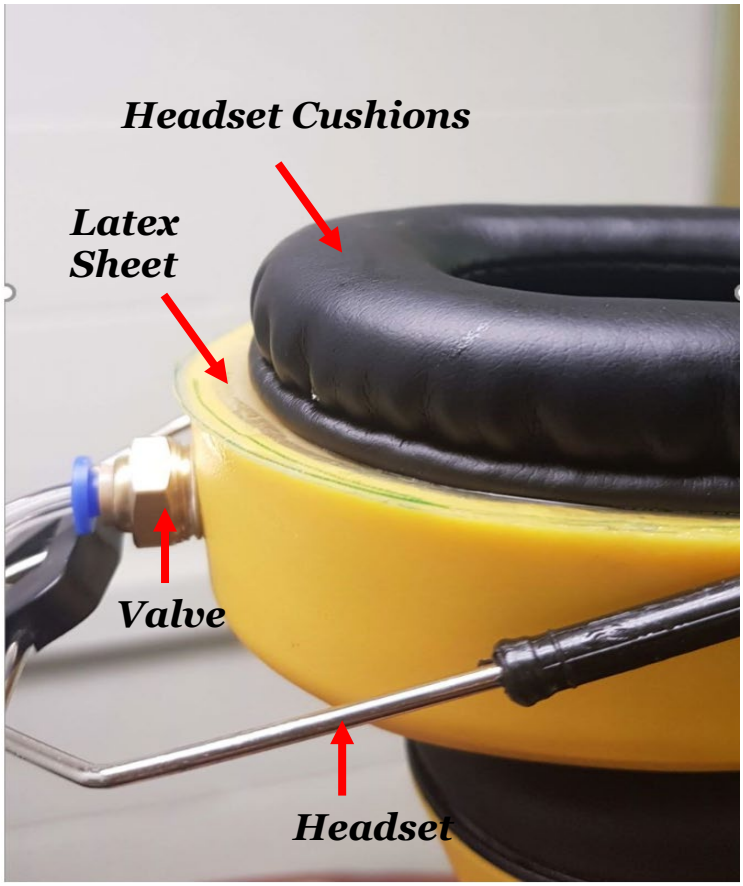

Figure 2.11: Headset setup

2.9 Summary

In this chapter, the basic system of the IAMM is introduced and the options for manufacturing the prototype are explored. The design philosophy of the prototype is explained with a part by part and step by step description. The design constrains of the IAMM are shown and the method used to overcome them are laid out including the method of fastening and the novel technique used to create air-tight seal. Allthe steps from pre-processing to post processing of each part are shown in this Chapter to clearly indicate how the apparatus was built. The extensive manufacturing knowledge used and implemented to create the perforations are explained and theair supply used for actuation is shown in this chapter.

Chapter 3: Performance Testing Of IAMM

3.1 Overview

When sound is incident on a body, usually one of three scenarios are possible:

Absorption – The sound is absorbed and dissipated as energy

Transmission – Sound can pass through the barrier body

Reflection – Sound is reflected off the barrier body

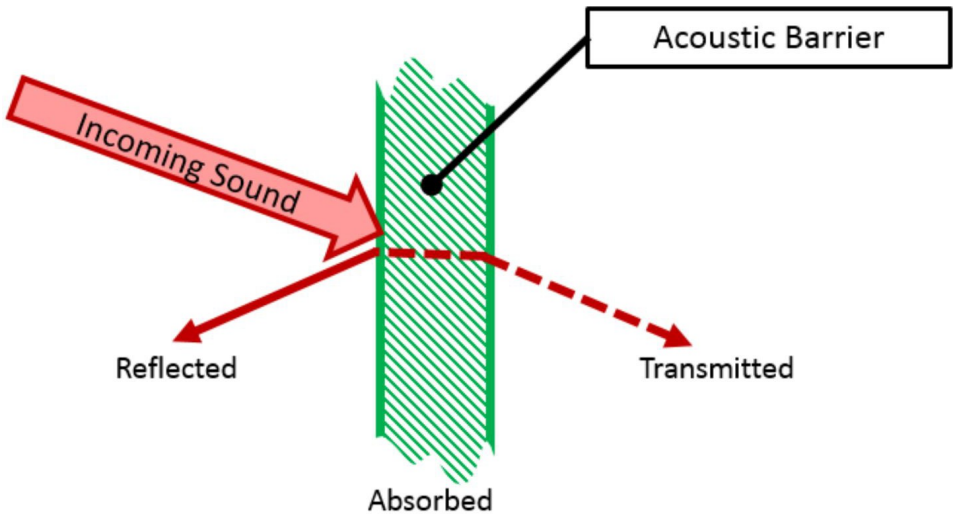

Figure 3.1: Wave propagation of sound through an acoustic barrier.

In the study presented, quality of sound treatment in terms of its transmission is investigated. Transmission Loss (TL) in general is described as the decrease in

intensity of waveform energy as wave propagates through a certain area or body of structure [37] . Sound Transmission Loss (STL) is used as a quantification of how much sound is prevented from passing through a sound treatment. It also provides a way to measure the effectiveness of acoustic treatments. Sound transmission loss (STL) is also defined as the ratio of sound energy incident on a sound treatment to the sound energy transmitted through the sound treatment [38].

$$STL = 10log\frac{W_i}{W_t} \tag{3.1}$$

Sound Transmission Loss (STL) is measured in decibels, which is the logarithmic ratio of the two energies. In heat analogy, it can be described as the decreasein heat flow. The Inflatable Acoustic Metamaterial (IAMM) prototype is essentially a sound treatment and hence it is imperative to find its Transmission Loss.In this study, the STL is measured in three scenarios, which are positive, neutral and negative control. Positive control signifies inflation of the metamaterial mem- brane, negative control signifies vacuum while neutral control is static. The STL in these different scenarios will help formulate a clear idea of the performance of the inflatable acoustic metamaterial (*IAMM*).

The result is usually plotted on a graph of Frequency vs decibel (dB). This is mainly because Sound Transmission Loss is a function of frequency. The y-axis is used to denote the amount of sound intensity absorbed by the sound treatment orin this case, the prototype. The design of the structure in the prototype is made in accordance to the mass-law that dictates its transmission loss. The perforation

in the prototype behaves like added mass and provides a compressible structure that facilities a dynamic behavior. This also provides us with an outlet to better understand how such structures and dynamism alters the transmission loss.

Sound Transmission Loss can be measured in two ways, either using the impedance tube method or the two-room method. In this study, an impedance tube is employed to determine the Sound Transmission Loss in various conditions while in the Two Room Method, the prototype is more in-situ fastened. It requires larger area and is more suitable for larger specimens. The sound source is in one room and microphones are in both the rooms to measure the difference in sound. The rooms are sound proofed on both sides except for a window on the wall where the specimen to be tested is wall mounted. Impedance tube in contrast is usuallyon a much smaller scale.

3.2 Impedance tube testing

Impedance tube testing is done to measure the transmission loss or coefficient of absorption of smaller prototype or specimens as well as ducts, mufflers, etc. There are various methods by which this very test can be conducted. For this instance, the measurement procedure adopted was the four-microphone technique based on the transfer matrix method, as described in ASTEM E2611-09 [39]. The testing is done on a soundproof metal tube with a sound source on one end and the prototype in the middle. The tube is made from thick steel to ensure no sound is transmitted through it radially. The impedance tube has an outer diameter of 74mm and an

inner diameter of 35 mm. This inner diameter is the prevalent value that we have taken into the design consideration. To measure the acoustic pressure difference inside the tube, four quarter inch pressure-field microphones are flush mounted on the tube walls. The microphones are paired on either side of the specimen and are equally spaced between each other by $L_1 = L_3 = 35mm$. Microphone 2 and 3, which are on either side of the specimen are spaced by $L_2 = 15mm$. This setup enables sufficiently accurate measure of sound transmission loss in the frequency range of 0 Hz to 5000 Hz.

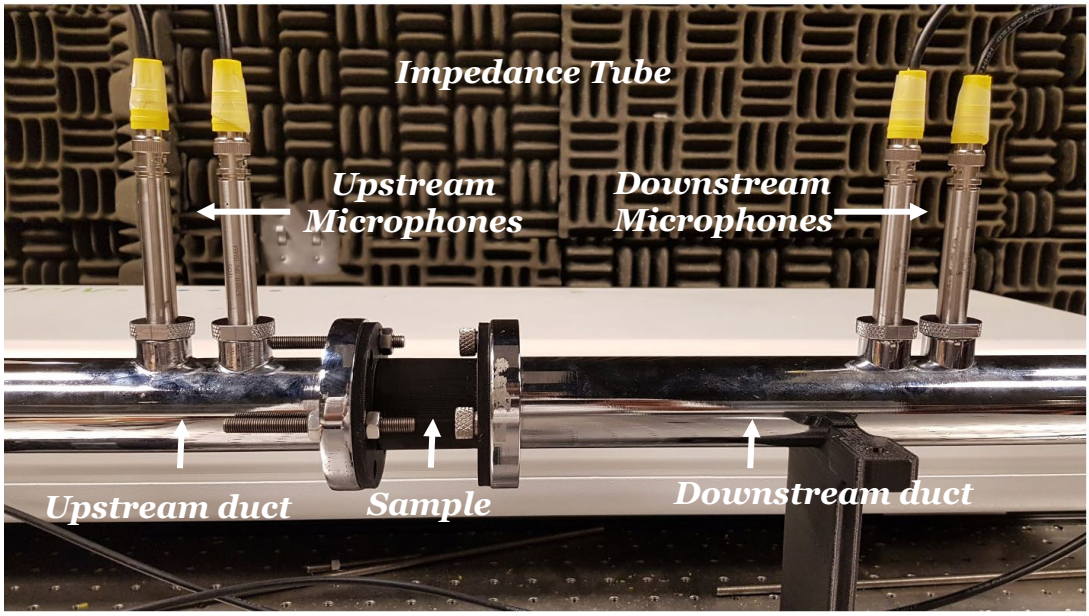

Figure 3.2: Typical Impedance tube setup with 4 microphones.

Since STL is independent of the source of the sound, any source can be used. The *ACUPRO* impedance tube set up, which was utilized for this study, contains a loudspeaker as the sound source on one end, driven by a white noise signal generator that generates plane waves that propagate inside the tube. The speaker is fastened to the tube in a fashion that ensures no air gaps. This makes sure that the sound is

concentrated and is always directed normally to the prototype fastened in the middle for testing. The tube before the specimen is called upward measurement duct and the tube after that ends in anechoic termination is called downward measurement tube.

The impedance tube set-up is mounted on equidistant supports that hold it steady on the vibration-controlled table. In order to ensure the fastening of the specimen, flanges are provided with threading in each which enable the use of screw bolts to fasten. The flanges in the specimen design make the mating more easier. In theory, the fundamental working of the impedance tube in this testing method is very elementary, as its employs the four-microphone transfer matrix method. There are two microphones before and two microphones after the prototype, which allows the pressure difference in the tube to be measured via which sound intensity can be calculated. This in turn is then used to find the transfer function.

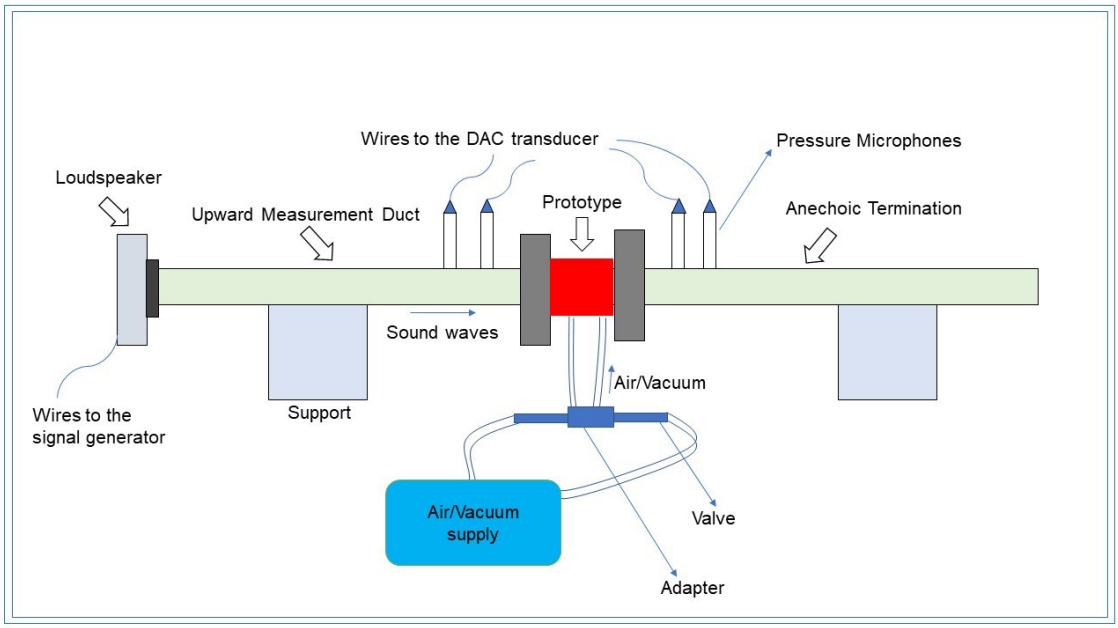

Figure 3.3: Impedance tube setup used for this study.

The experimental set up is controlled by the computer that runs the proprietary software, which is built on *LabView* kernel. The input signal is parlayed to the impedance tube by the computer. This process is facilitated by the transducer (Data Translation Model *DT9837A*). The transducer possesses data acquisition that converts the digital signal from the PC to analog for the impedance tube. The transducer itself is a series of electronic components. It has five ports, four for the respective microphones and one USB port for data transfer to and from the PC. The output connection is connected to the Loudspeaker at the end of the transmission tube. The loudspeaker is the source that creates the white noise signal normally tothe specimen. The transducer hence is an all-in-one electric component of the data acquisition, signal generator and the amplifier, thus allowing for a crisp and clear signal. The input that runs the signal generator is initiated by the user via the computer.

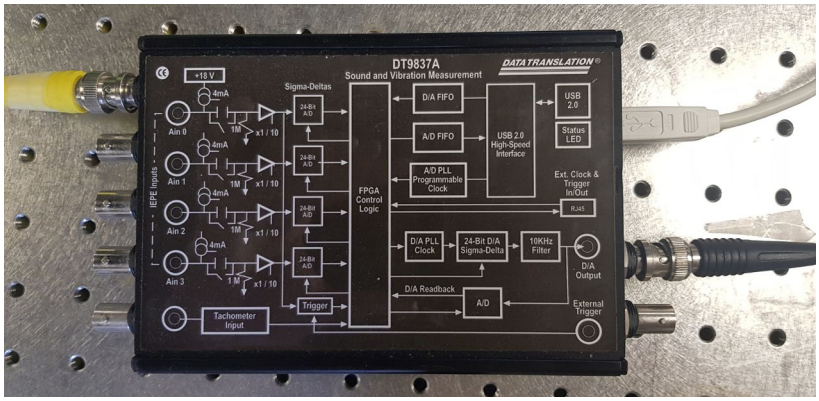

Figure 3.4: 4 channel USB Data Acquisition device.

The testing was conducted as per ASTM E2611-09, which instructs the usage two different termination per sample configuration to obtain the sample's transmission factor [28]. The terminations can be user defined, usually an open end

and a close end. In this study, the terminations used were (1) open ended termination and (2) loaded termination that uses a 25 mm thick stainless steel piston. For each sample configuration, the transfer matrix is calculated using:

$$T = \begin{bmatrix} T_1 & T_2 \\ T_3 & T_4 \end{bmatrix}$$

The specimen having a length of 55 mm is mounted onto the tube using screws to be fastened to the flanges. The specimen is placed in between microphone 2 and microphone 3. In order to be accurate in determining acoustic properties using the impedance tube, it is imperative that the microphones are in phase. Therefore, standard phase calibration should be conducted before running the tests. When tests are run, the computer initiates the signal generator to produce white noise frequency sweep in the required range, which is 0 -5000 Hz. The microphone then picks up the signal before and after the specimen in the impedance tube. The microphone signals are then collected with digital data acquisition in the transducer that is connected to the computer. The software in turn calculates the transfer function *H11, H21, H31, H41* by performing Forward Fourier Transform (FFT) on the acquired microphone data. The reference signal for the transfer function is given by microphone 1 [28].

3.3 Result of impedance tube testing

The acoustic performance of the inflatable acoustic metamaterial was tested in the impedance tube. Apart from the transmission loss characteristics, the stop

band behavior is also to be evaluated. As mentioned before, the apparatus was evaluated in three scenarios: neutral, positive and negative. These control scenarios reflected the type of actuation the metamaterial is subjected to with neutral being static while positive and negative being air pressure and vacuum, respectively.

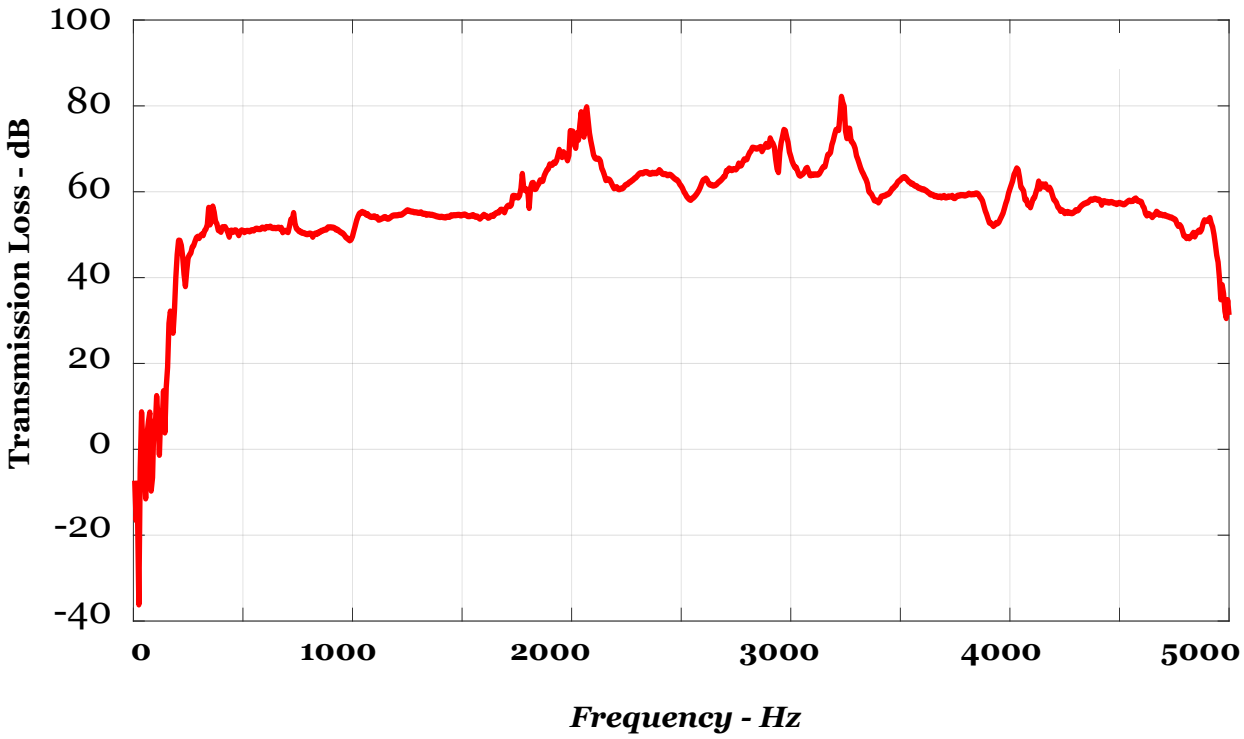

Figure 3.5: Transmission Loss behavior of IAMM in neutral control

The result graph shows the performance rating of the IAMM to be in the vicinity of 50-60 dB. The more standout part is the stop band in low frequency region of 500Hz-2000Hz. This indicates great performance in low frequencies. When subjected to air pressure the start perforations of the IAMM undergoes non-linear deformation. This causes change in geometrical stiffness of the membrane.

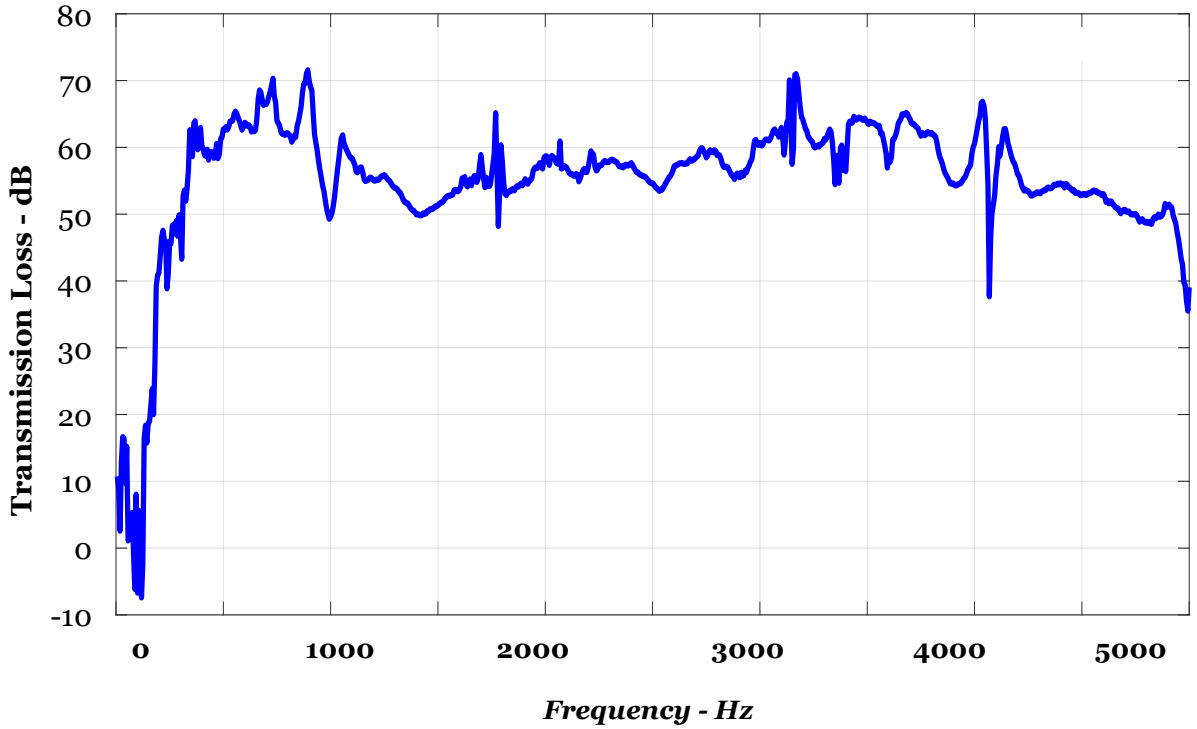

Figure 3.6: Transmission Loss behavior of IAMM in positive control

It is evident from the graph that in even lower frequencies range 0-1000 Hz, the positive control performs better in attenuating the noise. When the apparatusis subjected to vacuum pump for the negative control the noise attenuation characteristics alters. This is because, the suction produced inside the perforation forces it to come together and hence, increase the effective density in the path that the sound has to travel. In negative control, due to this increase in density and lack of travellingmedium, the transmission loss behavior curve is evidently absent of much of the resonance peaks that are visible in the other two conditions.

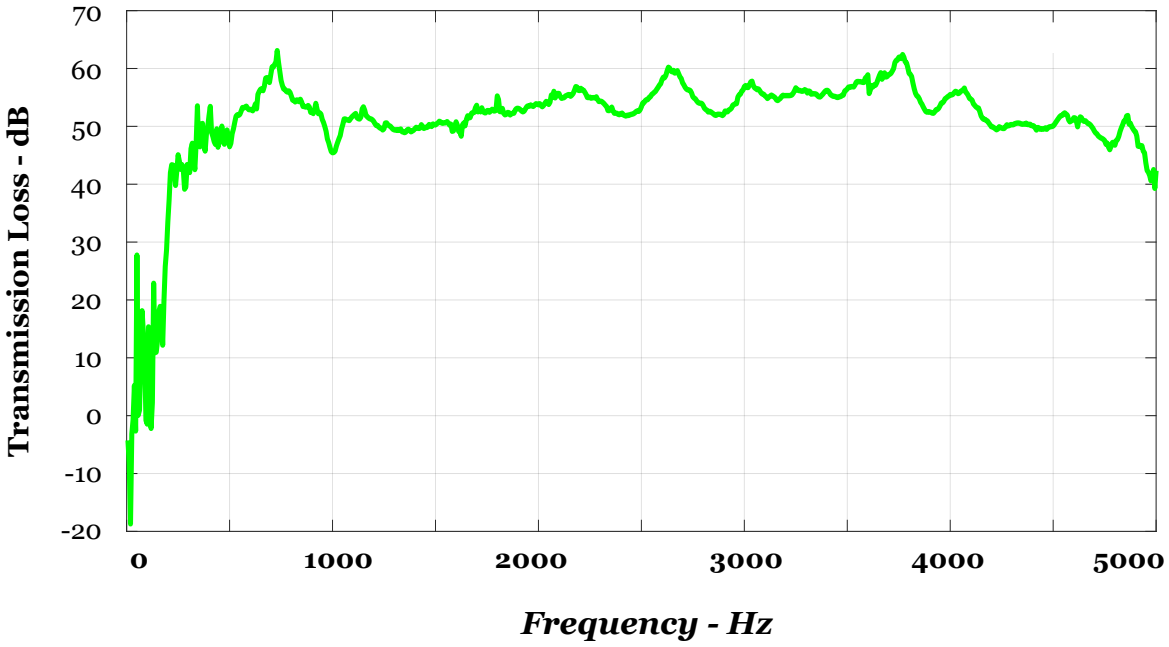

Figure 3.7: Transmission Loss behavior of IAMM in negative control

3.4 Frequency response test

To further understand the quality of the sound treatment proposed, real life instances of such a method should be verified. In order to do this, the IAMM is installed in an ordinary noise reduction headset. Thus, to attain clearer understanding of the performance of the IAMM in the headset, the overall quality of the modified headset should be verified. This is done by conducting a frequency response of the headphone, which in this case, a frequency sweep.

Frequency sweep usually generate a sine waveform that changes frequency with time. Start and stop frequency usually defines the limits of the frequency sweep. It is usually used for frequency response testing. In the context of acoustics, frequency sweeps are used to understand the acoustic characteristics of a room or an object [39]. It is instrumental in understanding reflective and sound absorption characteristics.

It generally serves the purpose of describing the time-dependent behavior of a sample in the non-destructive deformation range [40]. High frequencies are used to simulate fast motion on short timescales, whereas low frequencies simulate slow motion on long timescales or at rest. In practice, frequency sweeps are methods for gathering information on behavior and inner structure of polymers [40].

The frequency sweep is essentially a frequency response that can be explained as the difference of output and input. Hence, the frequency sweep is conducted between a range of frequencies and the input is measured before the sound treatment and the output measured after the sound treatment. These are then correlated with each other to obtain the response of a sound treatment.

3.4.1 Testing Apparatus

In this study the frequency response of the *IAMM* installed headset is done by utilizing a *KEMAR* manikin. *KEMAR* is a test device by G.R.A.S that can test any device that containing loudspeakers and microphones [41]. It is essentially an anthropomorphic head and torso manikin with adjustable neck and torso.It comes with modifiable pinnae as well as a modular pinnae hole that facilitates adaptability to any requirements. The testing manikin is bolted down to a thick steel plate for stability and adjustments. Inside the testing manikin, a condenser microphone is attached into the right pinnae hole. This microphone is used to measure the output sound for the frequency response.

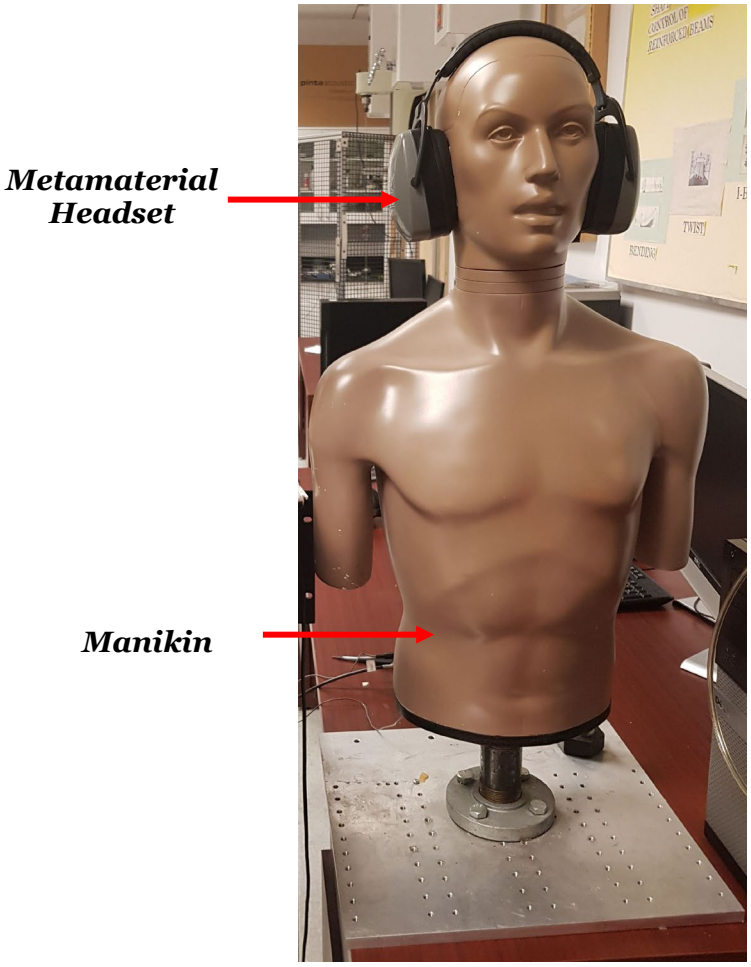

Figure 3.8: G.R.A.S KEMAR Testing Manikin [41].

The frequency response is conducted by running a frequency sweep in the range of 0-5000 Hz. This range corresponds to the range from the impedance tube. A function generator is used to create a sine sweep, a sine wave that changes the frequency from the start to the stop frequency. A vibration analyzer is used in this apparatus to both generate the function as well as read the outputs. Stanford Research SR785 Dynamic signal analyzer is the equipment chosen. It has two channels and is capable of conducting a multitude of vibro-acoustic testing [42]. It is also equipped with a dual output screen that enables reading two signals and displaying

them for easier representation. In this scenario, these channels enable showing the input and output readings in real time. This Dynamic Signal Analyzer (*DSA*) is used to produce and read a linear sine sweep in the aforementioned range. The *DSA* is essentially a combined unit of vibration, spectrum, network and octave analyzers with a built in oscilloscope [42].

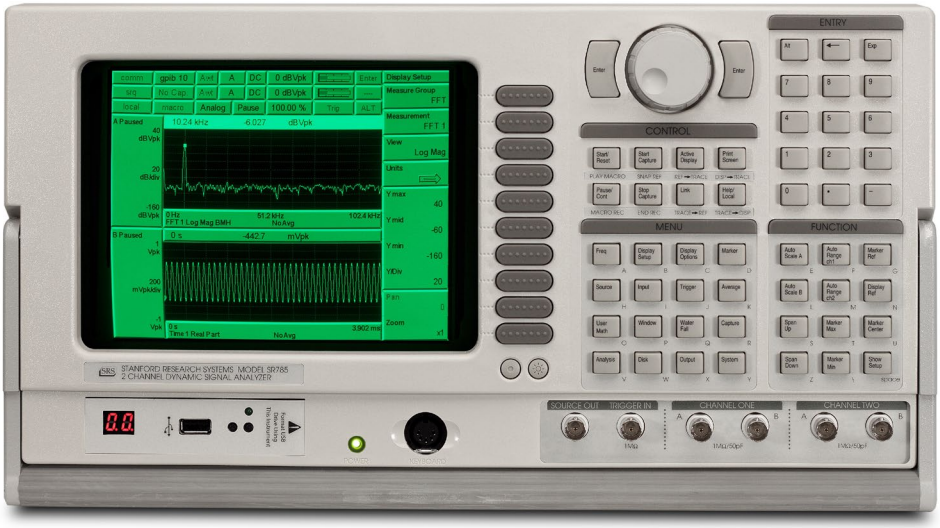

Figure 3.9: Stanford Research Vibration Analyzer SR785. [42]

The signal from the analyzer is sent to an amplifier to create a cleaner audible signal. The amplifier is utilized to create a signal whose amplitude is double folded. This is very imperative because the normal signal amplitude from the *DSA* is so small that it will be hard to separate the noise and see a cleaner output. The amplifier essentially is a conduit used to convert a weak line signal, the highest signal strength before amplification, to a strength that can be sent and used by the speakers. The boosted line signal from the DSA is then parlayed into a speaker to create the required input signal for testing. The speaker is kept in line with the ear

of the *KEMAR* test manikin to simulate a real life sound incident on the *IAMM* installed headset.

Figure 3.10: Wilcoxon Research PA7E power amplifier.

In order to measure the frequency response of the headset, we need both the output and input to the headset. The output for the frequency response is measured by the condenser microphone inside the manikin pinnae. The input signal from the DSA via the speaker is measured by a pressure microphone stationed outside near the speaker. The microphone is to be kept as close to the speaker as possiblein order to read the signal as accurately as possible. The pressure microphone produces a mic level signal. Mic level is the voltage of signal usually generated by a microphone and is the lowest, weakest level of signal. Therefore, the *DSA* is unable to read this signal clearly unless a pre-amplifier is used. Pre-amplifier is essentially a conduit used to bring the weak mic level voltage signal to the level of the input signal for the analyzer to read. The data from the vibration analyzer is then retrieved via the data storage system.

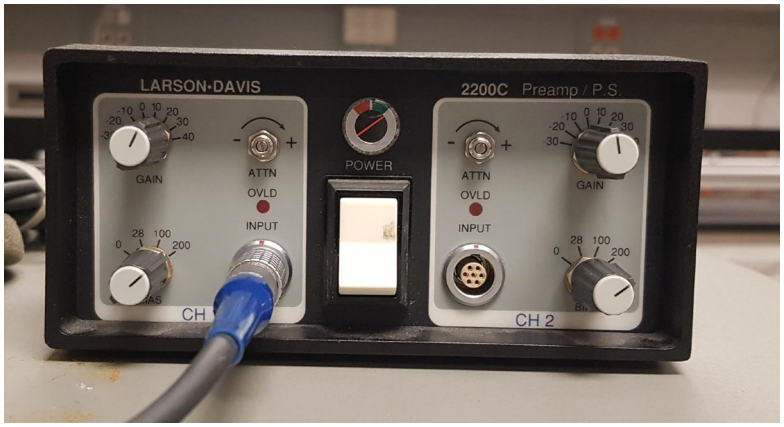

Figure 3.11:Larson-Davis dual channel pre-amplifier.

The transmission loss of the *IAMM* installed headset is then calculated from the data retrieved by the vibration analyzer. *MATLAB* is used to convert the SPLand create the transfer function and plot the necessary graphs.

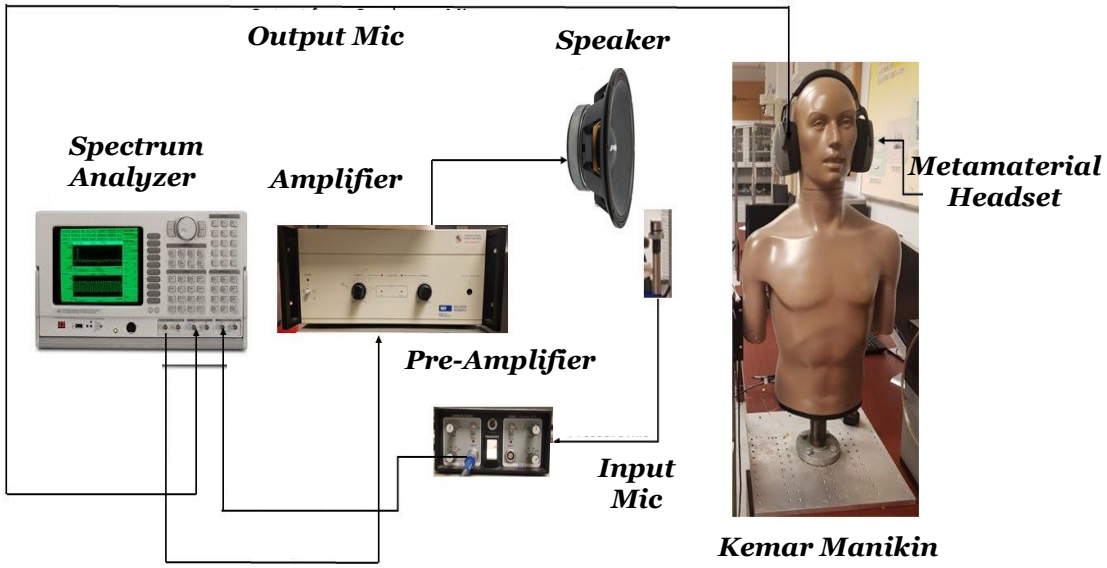

Figure 3.12: Experiment setup block diagram.

3.5 Results of frequency response.

The frequency sweep is done from 1Hz to 5 kHz with 56.6 s second time scale at each frequency. Similar to the impedance tube testing, the headset was conducted in three control scenarios. The transfer function was extracted from the *DSA*. The same 6V vacuum pump was used for the actuation of IAMM inside the headset.

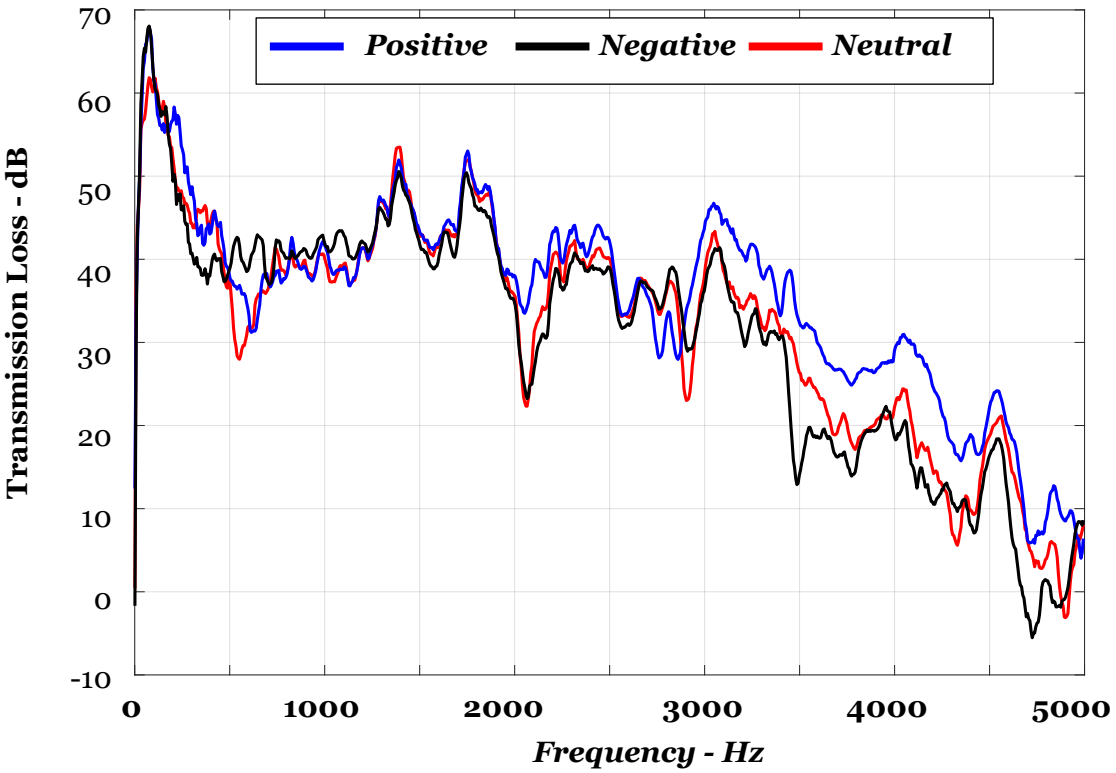

Figure 3.13: Experiment setup block diagram.

It is evident from the above graph that, in the lower frequency region the IAMM installed headset seems to fare favorable as compared to the higher frequency ranges across all three scenarios. When actuated positively or negatively from the performance graph it can be deduced that in certain regions of frequencies, higher transmission loss can be created from the neutral control.

In the regions 500Hz-1250Hz, negative control performs favorably higher than the other scenarios. While in between 2500Hz to 5000Hz positive control is considerably higher than other two controls. This higher transmission loss is favorable.

3.6 Summary

This chapter goes across all the experiments that are used to validate the performance of the *IAMM*. The Transmission Loss of the *IAMM* is evaluated using *ACUPRO* impedance tube in three neutral, positive and negative control scenarios. These scenarios are adjudged by the kind of actuation produced in the *IAMM*. The *IAMM* is also installed in a headset to understand the true actuation of the sound treatment. This performance is done by getting frequency reasons during a sine sweep using a *KNOWLES* manikin setup. In this chapter the results from all of these different tests provide a snapshot overview of how the *IAMM* facilities sound attenuation in the range 0-5000Hz.

Chapter 4: Finite Elemental Analysis of IAMM

4.1 Overview

Finite Elemental Analysis (*FEA*) of *IAMM* was conducted using *ANSYS*. It is a process of running a simulation of physical phenomenon using numerical methods of *Finite Element Modelling* (*FEM*). This *FEA* software package enables the utilization of various subsystems to simulate physical phenomenon in multiple domainsof engineering using numerical methods. In this study, the availability of acoustic subsystems was utilized to run harmonic analysis of the acoustic metamaterial. Multiple subsystems were run in conjunction with each other due to the need of an evaluation the pre-stressed state. In *FEA,* a smaller the size of the element, more accurate the final solution. This comes with a caveat of being computationally expensive, hence it is imperative that a fair trade off be found in terms of element size and the computational time.

To clearly study the acoustic performance and parameters of the *IAMM* prototype, modal and harmonic analysis were conducted. Modal analysis helps in generating modes and mode shapes. These are essentially directly related to the natural frequencies of the structure. Harmonic analysis creates a harmonic sine sweep excitation and evaluates the model on how it reacts to the excitation.

4.2 Modal Analysis

Modal analysis is the study of dynamic properties of a system in the frequency domain. It converts the measured vibration signals of excitation (input) and responses (output) of a complex structure that is usually hard to visualize, intoa set of modal parameters. It provides an overview of the limits of response of a system. Here, modal analysis helps in retrieving the natural frequencies and mode shapes. The natural frequencies are then used to retrieve eigen-values and eigen- frequencies. This essentially helps in a better understanding of the dynamic characteristics of the metamaterial. Modal analysis is usually done to extract free vibration responses of the system. The 'modal' subsystem from ANSYS is used to run the analysis.

Figure 4.1:Modal subsystem in ANSYS

In this study, the modal and dynamic characteristics of the metamaterial system were deeply studied. The unit cell perforation was first analyzed by using

the *FEA* package of *ANSYS Workbench 19.1*. Modal analysis was conducted on both the unit cell as well as the extended metamaterial structure. After extracting the modes and mode shapes, further analysis was done in the pre-stressed conditionsof inflation and deflation.

4.2.1 Unit cell

The acoustic metamaterial is essentially a periodic tessellation of unique unit cells. Hence, to truly understand the physical phenomenon and dynamic behavior of the metamaterial, the unit cell used to create the tessellation is to be studied.The unit cell encompasses the tetrahedral nodes and the perforation. The modal analysis simulation is run in both unstressed and pre-stressed conditions. This wouldhelp in extracting the mode shapes of the unit cell in different excitations. The modal analysis is done for up to the initial 10 modes.

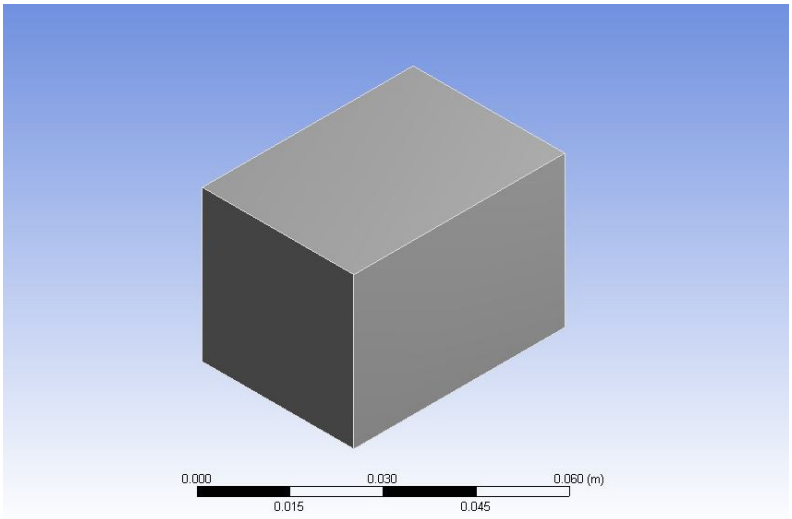

Figure 4.2: Unit cell model

The unit cell 3D CAD is made using Autodesk Fusion 360 software package and

is imported to *ANSYS*. The interior tetrahedral perforation and the outer cases are assigned their respective material of Agilus-30 and poly-carbonate plastic. Modal analysis does not require much initial conditions as they are assumed by the program and hence program controlled. The initial conditions prescribed before the analysis are the connections of the unit cell and its boundary conditions in terms of supports. The connections are set as joints with rigid fixations. The joints are the tangential links from the nodes that connect to the outer edge and are set to rigid as there are absolutely no movements between the faces.

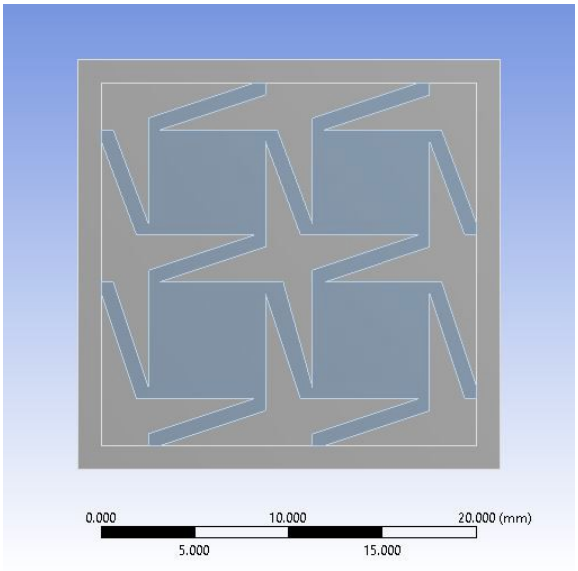

Figure 4.3: **Sectional view of unit cell model exposing the tessellation**

In order to reduce the computational time, the solver's default size was used to discretize the mesh for the model. The mesh is then evened out by using edge sizing. The whole unit cell structure is then constrained by fixing the top and bottom edges to avoid movement.

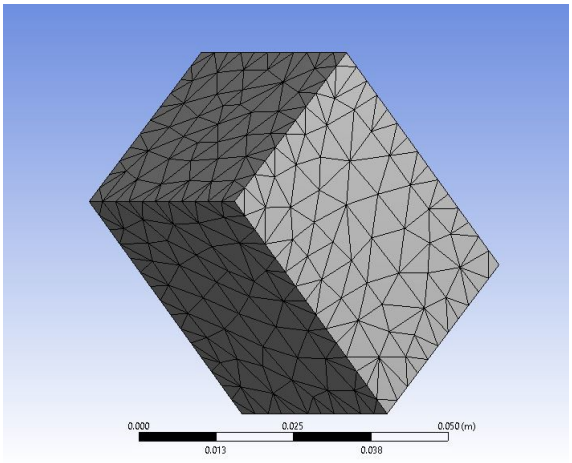

Figure 4.4: Discretized mesh of the unit cell

4.2.2 Inflatable acoustic metamaterial

To have an adept understanding of the behavior of the acoustic metamaterial,it is imperative that the study of the final prototype be conducted concurrently with unit cell simulation. The aforementioned steps are also adopted to conduct modal analysis of the prototype. The simulation was yet again conducted in positive andnegative control for the prototype.

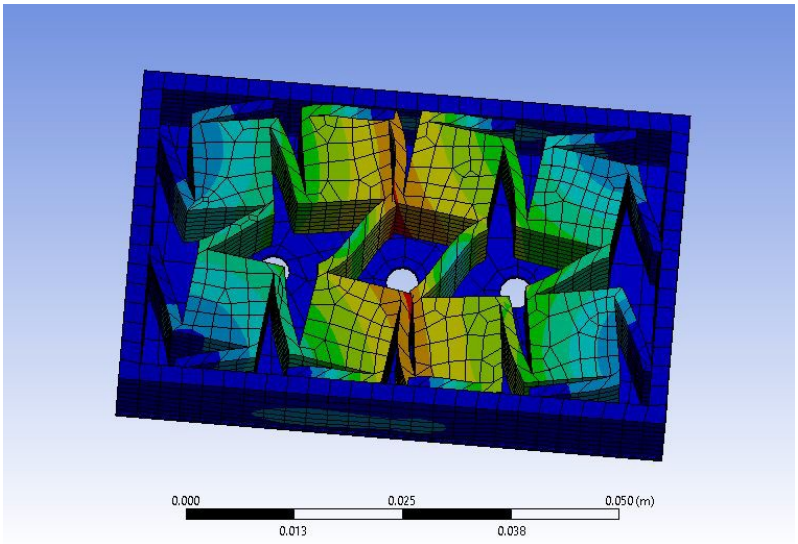

Figure 4.5: Positively stressed prototype.

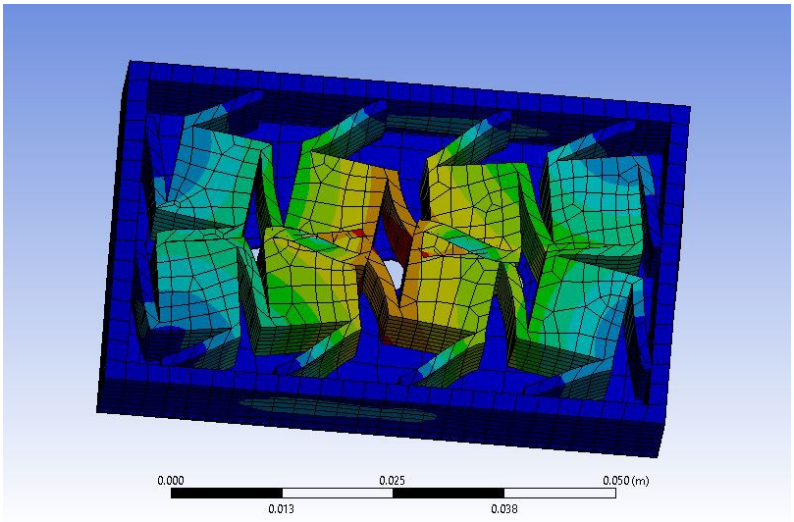

Figure 4.6: Negatively stressed prototype.

This helps in the understanding of how the repeated tessellation of the unit cell perforation would change its modal frequencies. The idea behind the periodic repetition is that non-uniform deformation of multiple perforations would be able to create a broadband resonance band.

4.2.3 Static structural

In order to simulate the deformation, the prototype would face, the unit cell of the tessellation is undergoes the same deformation. The unit cell is subjected to pressure force. The load is applied in sub-steps that are program controlled. The steps for the simulation are fairly straight forward. The unit cell is constrained in terms of the movement using fixed support on the edges that mirror constraints from the impedance tube.

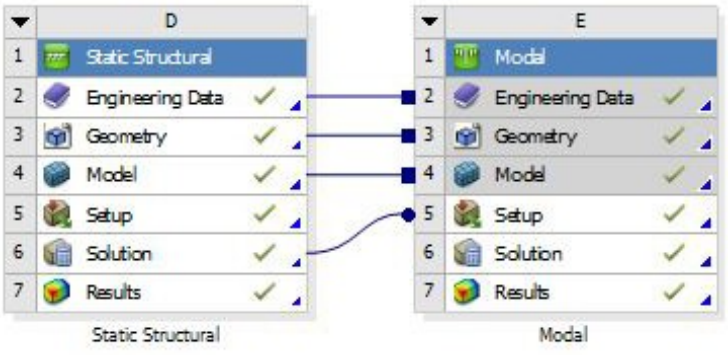

Figure 4.7: Static structural coupled with modal analysis.

The boundary conditions are similar to the unstressed modal analysis. The unit cell is constrained by the edges to restrict movement. The pressure is appliedon the insides of the perforations. Pressure load of 15000 Pa is applied to cause the tessellation to deform. The deformed model from the last sub step is used to conduct the modal analysis in the pre-stressed conditions. This enables the extraction of the modes and mode shapes. The pre-stressing should shift the modes that are the natural frequencies of the structure. Resonance is said to occur near the mode frequencies and hence by displacing it via pre-stressing, a workable range of resonance can be obtained.

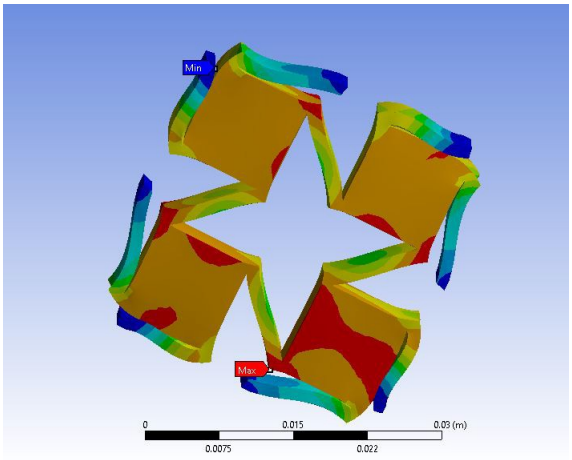

Figure 4.8:Unit cell undergoing positive deformation.

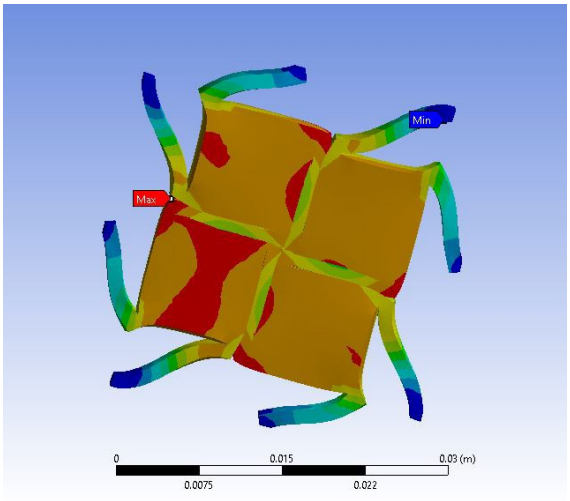

Figure 4.9: Unit cell undergoing negative deformation

4.2.4 Results

The modal analysis was conducted up to the first 10 mode and mode shapes. This is due to the fact that the performance of the IAMM in low frequency range is the point of interest here. The first 10 modes of the unit cell when not in stress ranges from 43Hz to 223Hz. This would ideally correspond to the resonance peak in performance seen in the last chapter.

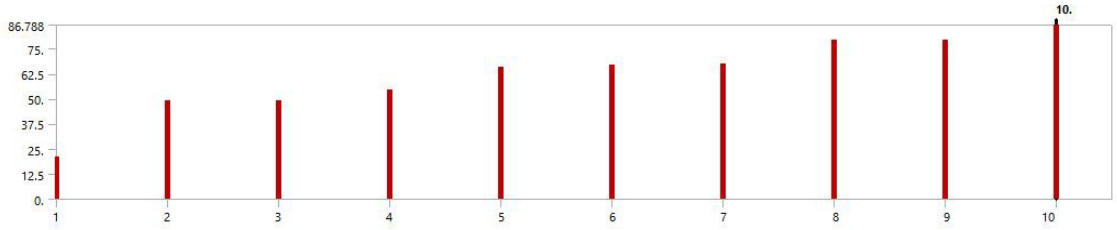

Figure 4.10: Modal frequencies of unstressed unit cell

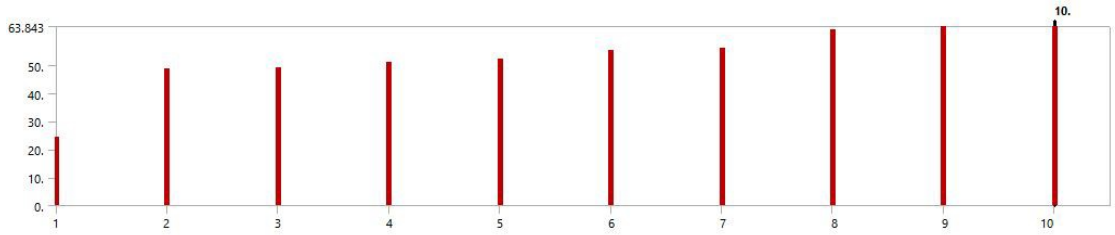

Figure 4.11:Modal frequencies of positively stressed unit cell

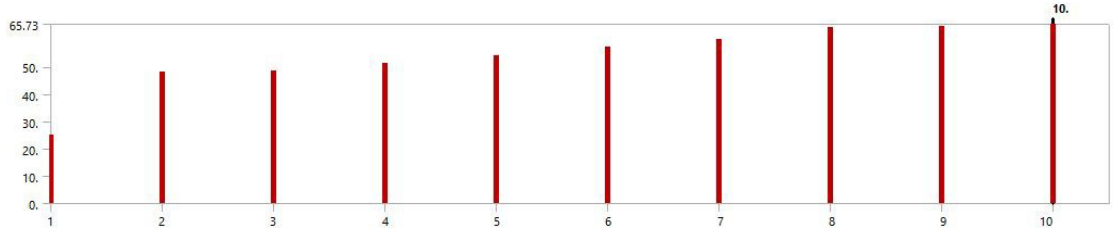

Figure 4.12: Modal frequencies of negatively stressed unit cell

MODES	MODE 1	MODE 2	MODE 3	MODE 4	MODE 5
Unstressed	20.801	48.811	48.981	54.519	65.833
Positive	24.45	48.808	48.808	51.217	52.251
Negative	25.077	48.393	48.548	51.274	54.323

MODES	MODE 6	MODE 7	MODE 8	MODE 9	MODE 10
Unstressed	66.873	67.35	79.149	79.292	86.788
Positive	55.288	55.918	62.86	63.818	63.843
Negative	57.248	60.341	64.689	65.058	65.73

Table 4.1: Comparison of unit cell modal frequencies

It is imperative that the mode participation of the modes are explored to truly understand the impact of the low frequency modes. The modal participation factor is mathematically defined as the product of mass times the mode shape in the given direction. It helps us in understanding the relative contribution of system modes to the system states. Therefore, the mode participation factor is better understood by evaluating the cumulative and the effective mass ratio.

When the unit cell is pre-stressed, the mode frequencies range from 73Hz to 161 Hz. Hence, it can be deduced from the simulations that the modal frequency range has been decreased from the static condition. When investigating the mode participation factor, it is evident that when pre-stressed, the mode participation factor of the system is more prevalent in the first three modes in the x direction and the first two in the y direction.

These modal frequency sets from the simulation of the unit cell shed light on the behavior when the unit cell is tessellated and hence the performance of the metamaterial can be evaluated. When unstressed, the first 10 modes of the printed prototype ranges from 48Hz to 141 Hz.

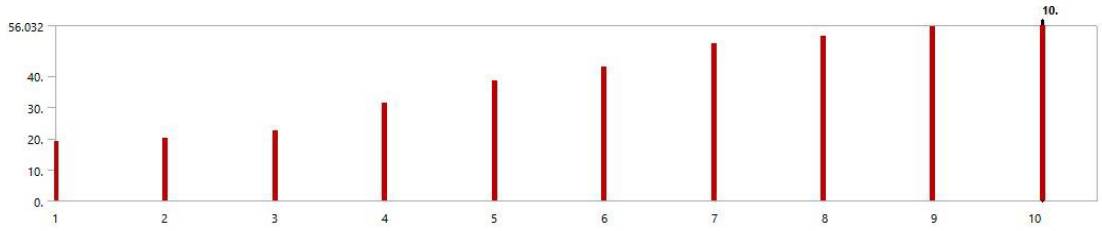

Figure 4.13: Modal frequencies of unstressed prototype

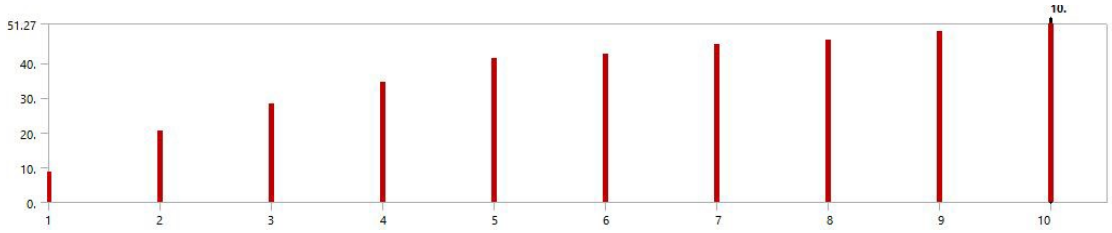

Figure 4.14: Modal frequencies of positively pre-stressed prototype

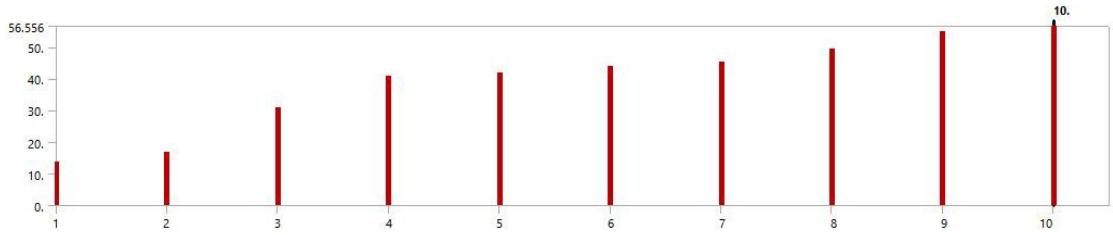

Figure 4.15: Modal frequencies of negatively pre-stressed prototype

MODES	MODE 1	MODE 2	MODE 3	MODE 4	MODE 5
Unstressed	18.95	19.982	22.515	31.13	38.329
Positive	8.6754	20.504	28.171	34.337	41.194
Negative	12.816	18.283	30.994	40.667	41.667

MODES	MODE 6	MODE 7	MODE 8	MODE 9	MODE 10
Unstressed	42.625	50.169	52.704	55.586	56.032
Positive	42.569	45.361	46.733	49.171	51.27
Negative	43.756	45.254	50.489	56.263	56.556

Table 4.2:Comparison of prototype modal frequencies

As the structure is pre-stressed, it is evident from the simulation that the set of modal frequencies are altered. When expanded or positively pre-stressed, the first mode shifts to 72Hz from 48Hz while the 10 mode is lesser than in the case of the neutral control. Conversely when the structure is negatively pre-stressed, the 10th mode is seen to shift higher as compared to the neutral case. The clustering of the modes also show significant changes when stressed.

4.3 Harmonic analysis

In harmonic analysis, the loading and the response of the structure is are assumed to be harmonic and cyclic. In this type of analysis, the a cyclic load directly propositional to sine function is applied on the structure to extract the system's

response. In order to simulate the impedance tube testing scenario, an acoustic excitation is applied on the system and the resultant Transmission Loss is recorded. Just like the modal analysis, harmonic analysis is also done under three conditions. A static acoustic subsystem is employed to create the necessary deformation in the structure before running the harmonic analysis to simulate the positive and negative control.

Figure 4.16: Harmonic acoustic subsystem in ANSYS

Unlike the modal analysis, the prototype structure when modelled in Autodesk Fusion 360 has to be modelled with the impedance tube inlet, outlet as well as the air contained within the structure. The metamaterial structure is assigned as Agilus 30 while the case is assigned Polycarbonate. These serve as the structural physical bodies of the components. Other parts, *i.e.*, the impedance tube ports and the body encompassed, are assigned air and hence are the acoustic bodies.

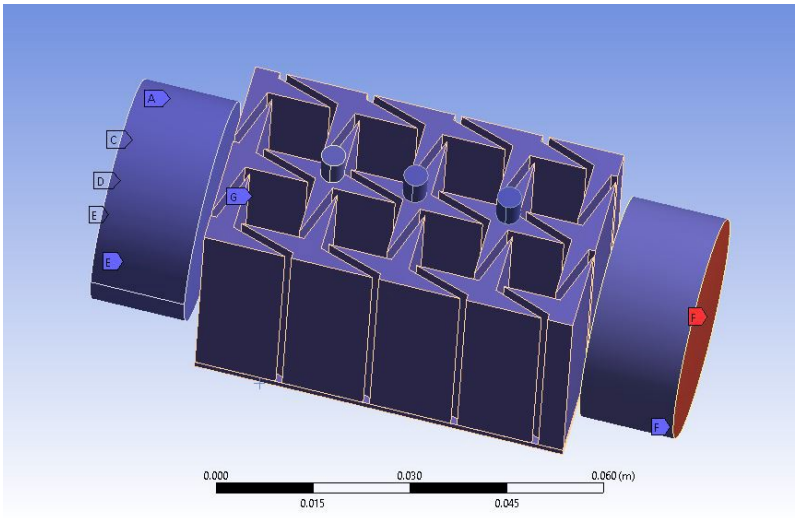

Figure 4.17: Air entrapped in structure and tube defined as acoustic bodies.

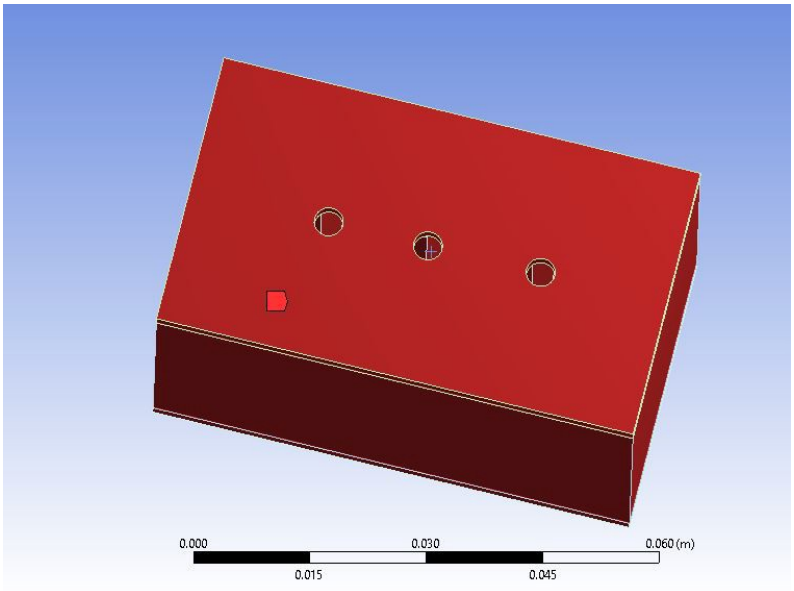

Figure 4.18: Other bodies are defined as structural physical bodies on themodel

Boundary conditions are then applied on both acoustic as well as physical standpoints. The structure is supported on the ends by securing it using fixed support. This will simulate the bolt fastening used to clasp the prototype to the impedance tube. The support is applied on the edges by using the line command

rather than the face command as the actual flange is omitted from the simulation since it doesn't intervene in the line of the impedance tube. In order to negate the back flow of sound that might be simulated because of sound bouncing off the ends, radiation boundaries are assigned to the tube ends as well as the orifice provided on the structure for the airflow. Radiation boundary conditions are assigned in order to give the property that wave motions from the interior incident on the boundary is to pass through with minimal reflections.

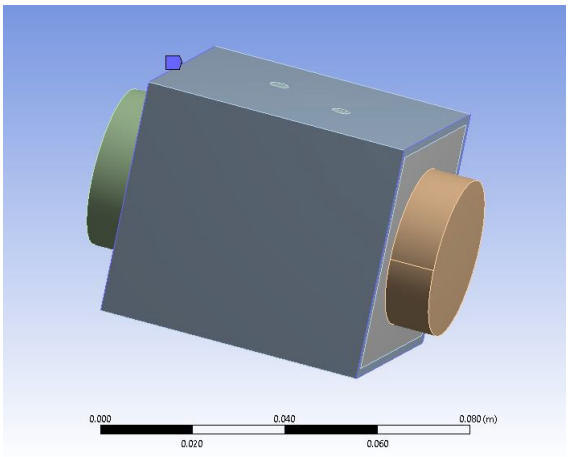

Figure 4.19:Fixed support defined on the edges

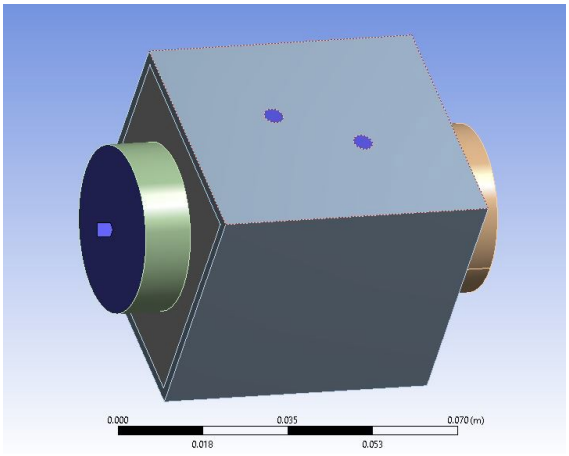

Figure 4.20: Radiation boundaries are defined on the ends to avoid soundreflected to be calculated.

In order to simulate the impedance tube, a frequency sweep is to be given as the acoustic excitation. Since the harmonic subsystem applies the load sinusoidally for the frequency range, the acoustic input should be designated by the frequency range and speed of sound. In ways of finding a trade off with computational time and accuracy, 0 to 5000Hz sweep was done in halves. The analysis was conducted between the range of 0-5000 Hz and 400 data points were extracted in between. Acoustic excitation was simulated by providing a mass source on the input inlet with a magnitude of 0.0024 Kg/ms. The acoustic body assigned to the impedance tube is appropriately assigned as port 1 for inlet and port 2 for outlet. The transmission loss is measured between port 1 and port 2 with the acoustic excitation in port 1.

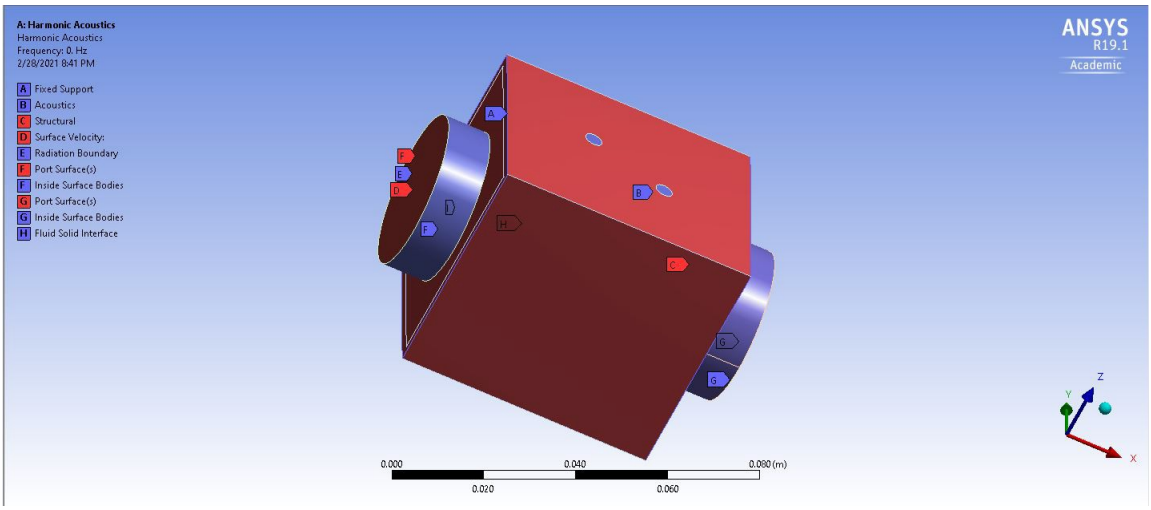

Figure 4.21: All the defined parts with impedance tube ends assigned as ports.

The discretization of the prototype again comes with the caveat of computational time if the elements are too small. The meshing is done by quadratic elementswhere an upper limit was adopted for the mesh size to decrease the number of elements. The math adopted to identify the mesh size for a quadratic

element is$\frac{\lambda}{}$. The mesh size is taken relative to the wavelength to accurately discretize the model. Since the computation was done in parts the mesh element size was adjudged to be 1.1cm or 0. 011m.The acoustic load applied was 2-way Fluid Structure Inter-action (FSI). The area that is in contact between the acoustic body and structuralbody is taken as FSI. This helps the solver to parlay both the displacement and force between the two .

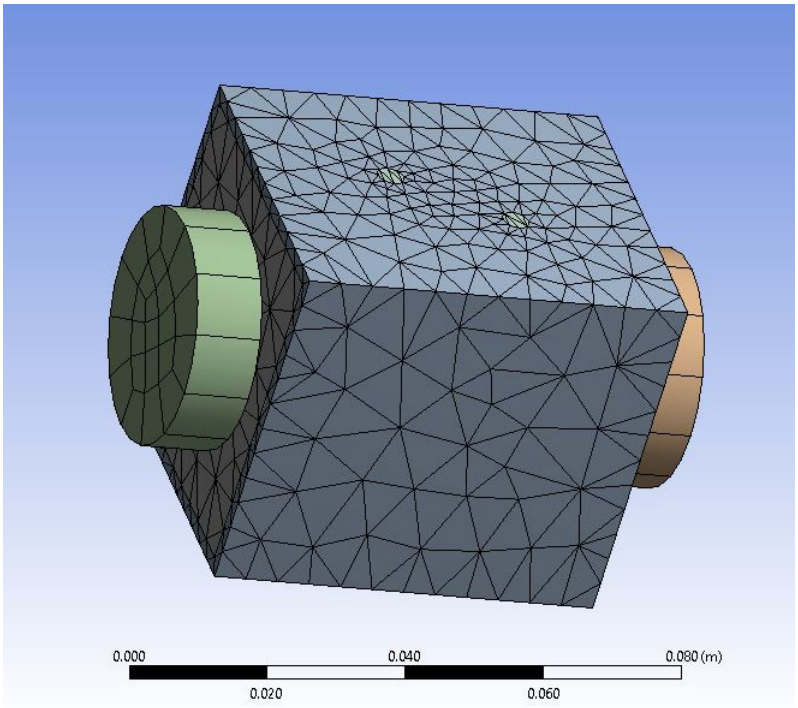

Figure 4.22: Model discretized by λ/12 as mesh size

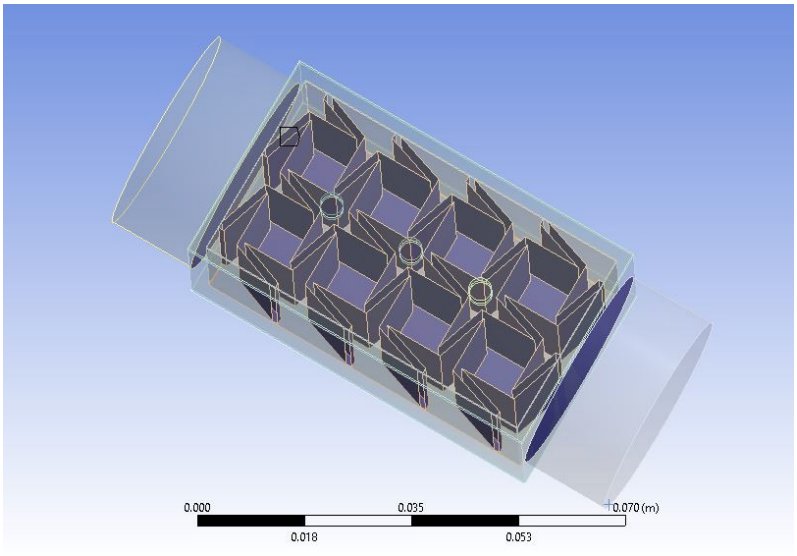

Figure 4.23: Fluid Surface Interaction (FSI) of the model

4.3.1 Static acoustics

In order to simulate the positive and negative control, static acoustic is to be employed in connection to simulate load bearing on the structure. Load is applied to make the structure contract and expand depending on the control required. The coupling of the static acoustic to the 2-way FSI coupling enables the solver to impart both the displacement and force.

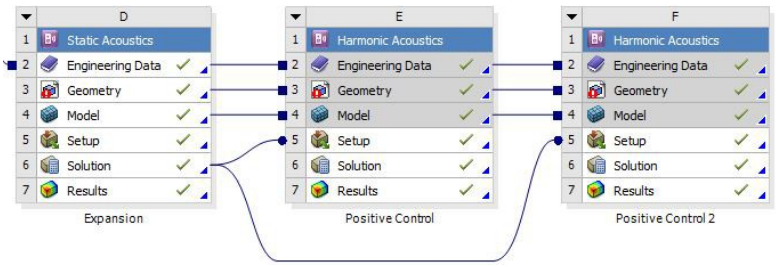

Figure 4.24: Harmonic acoustic subsystem coupled with Static Acoustic inANSYS

The initial conditions, like mesh size and material selection, are used similar

to the neutral control. The displacement constraint is then defined in the static acoustic rather than the harmonic acoustic analysis. The prototype is constrained by fixed support on either edges similar to neutral control. The load is then applied on the face of the star perforation ramped up in multi-step order that is program controlled. The load applied is 15000 Pa (2.5 psi) in steps. The total deformationis then extracted from the static acoustic solver. The deformed state is then usedto conduct the harmonic analysis.

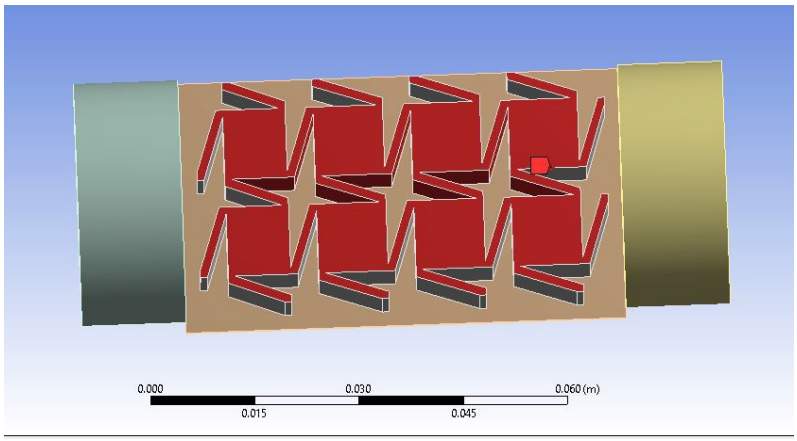

Figure 4.25: Pressure is applied normal to the face, the 2-way FSI couplingenables the imparting of the load

In the positive control, the pressure load causes the prototype to deform non-uniformly causing the chiral rotation of the tetrahedral. This type of deformation exhibits negative Poisson's Ratio. This pre-stressed deformation is then used to run ordinary harmonic analysis to simulate the positive control setup on the impedance tube. In the case of negative control, the pressure direction is just reversed to create a vacuum like load.

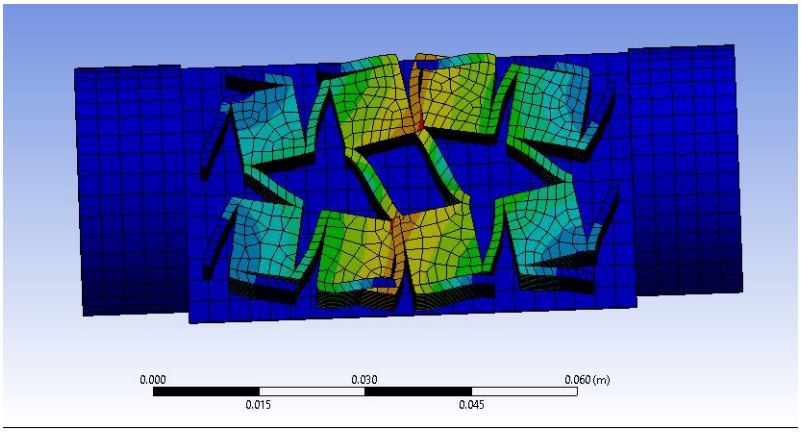

Figure 4.26: Simulation of inflated state caused by non-uniform deformation

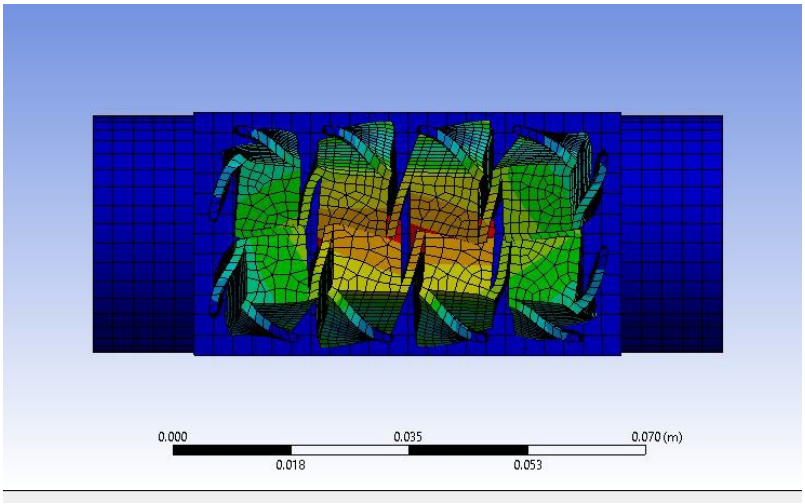

Figure 4.27: Simulation of vacuum state caused by non-uniform deformation

4.3.2 Results

The transmission loss for the frequency sweep is plotted on a Frequency vs Decibels (Db) graph. The results are measured in between inlet port, which is port 1, and the outlet port. In between the range, 800 data points are recorded for accuracy as well as to correspond correctly to the impedance tube data. The transmission loss is measured by the sound pressure level in the outlet port compared to the inlet

port. The transfer function is then extracted to calculate the Sound Transmission Loss (STL).

The input is a frequency sweep from 0Hz to 5000Hz to mirror the impedance tube excitation.

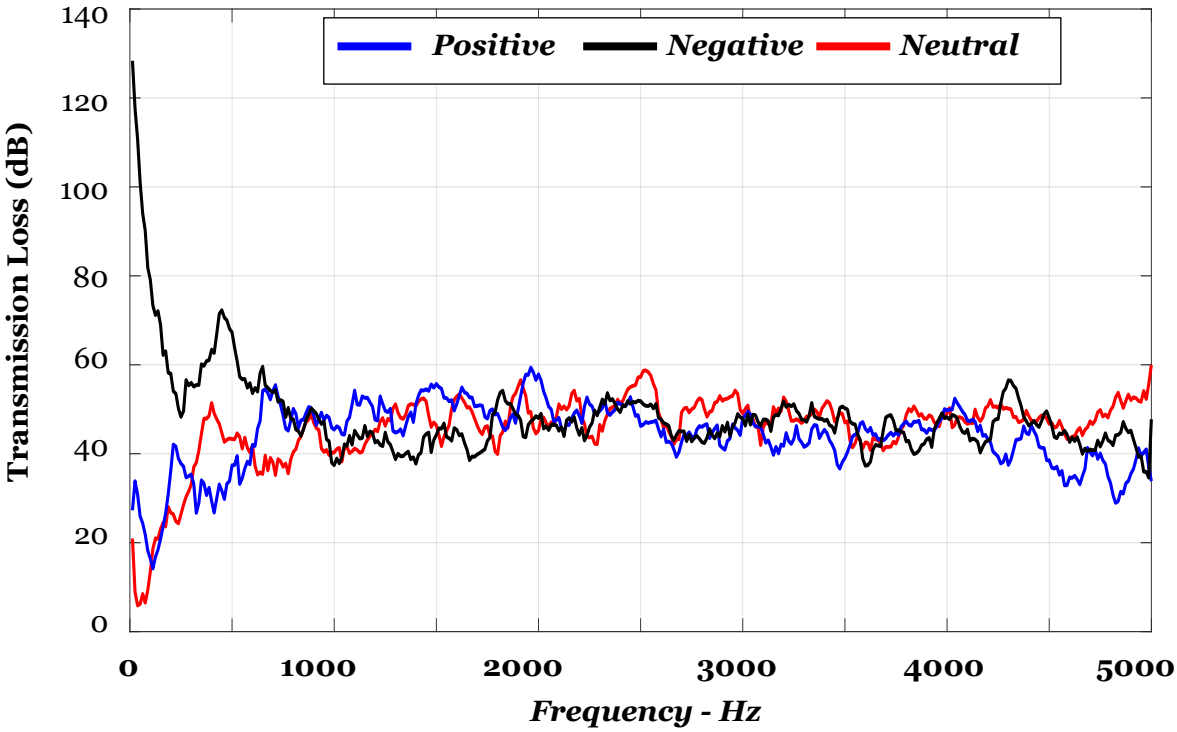

Figure 4.28: Transmission Loss comparison of the three control

The Transmission loss of all three control scenarios are determined and then plotted from their Excel data sheet using MATLAB. This enables in establishing how the transmission behavior of the metamaterial starts to alter according to the deformation in it. From the resultant graph above, it is evident that just like how the modal frequencies shift, the transmission behavior also translates. Transmission Loss behavior of the Inflatable Acoustic Metamaterial (IAMM) on being prestressed changes in the low frequency region. This was foreshadowed in the modal

analysis, as the modal frequencies of the prototype seemed to be lowered when prestressed. In the higher frequency range, it was noted that the transmission loss of the IAMM when pressured seems to lower considerably.

4.4 Summary

In this chapter the Finite Element Analysis (FEA) simulation results, conducted concurrently with the experiments are evaluated. Modal and Harmonic analysis was conducted for all three control scenarios for both the unit cell as well as the prototype. In this chapter, the modal frequencies extracted from the unit cell and the prototype was compared in order to facilitate clearer understanding of the control scenario behaviors. The simulation setup was delved thoroughly from discretization of the mesh to the boundary conditions applied in each simulations. Harmonic simulations were done to recreate the impedance tube tests. The chapter explains the kind of actuation the perforation should ideally undergo and how they will perform in the impedance tube. The results are then clearly compared with each other in this chapter.

Chapter 5: Comparison between Theory and Experiments

In order to understand the true nature of such an acoustic metamaterial, the deviant nature of the actual experimental behavior from the simulated results should be investigated. There will be always some discrepancies when comparing the theoretical and experimental output of such performance testing, this is mainly attributed to certain forces that are usually neglected when simulating. The FEA package extracts the data points when simulating at a point by point basis and hence, it is quite hard to precisely get the same results as the experimental.

5.1 Neutral control

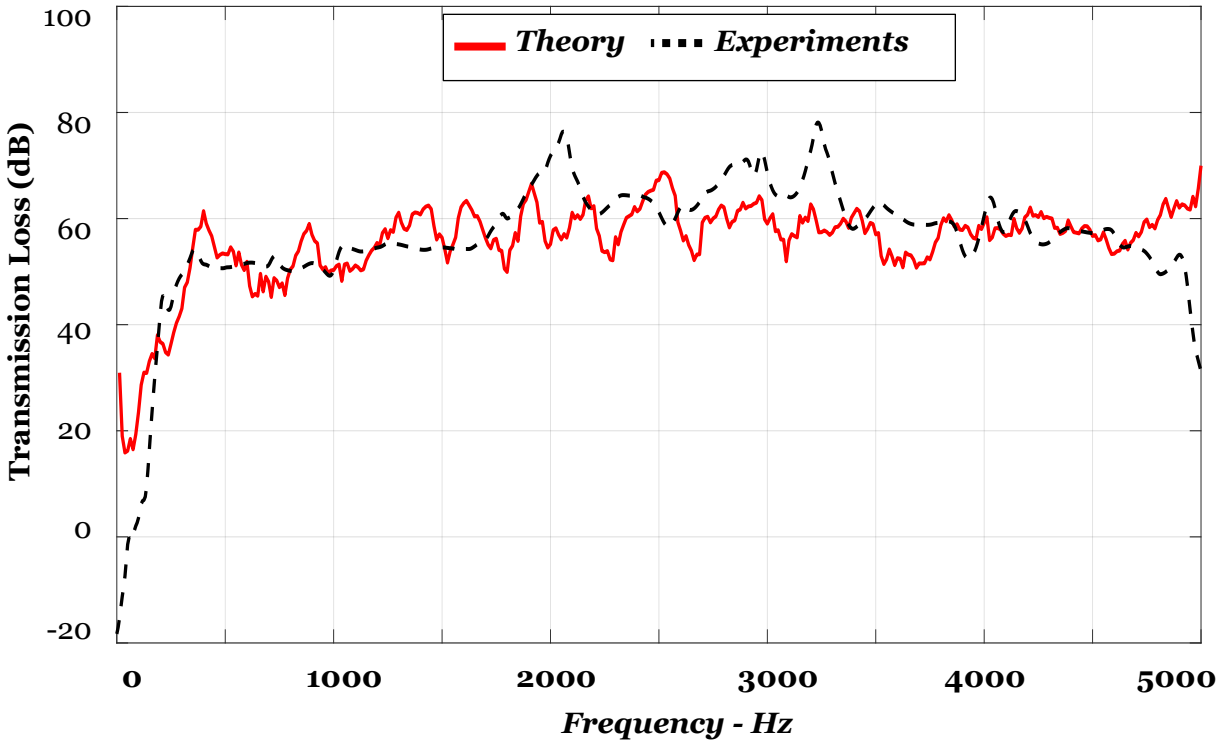

Figure 5.1: Comparison of theoretical and experimental performance of IAMM in neutral condition

In the small frequency range less than 500Hz, the results are usually very hard to converge due to the inefficiency of the simulation estimation to run such an analysis without being computationally taxing. The stop band behavior presentin the experiment cannot be seen in the simulation results. In the mid-range of the frequency spectrum that was investigated, the experimental performance seem to exceed the theoretical evaluation. The simulation model produced resonance peaks that was in reality is modulated and contained, thereby creating a stable stop-band.

5.2 Positive control

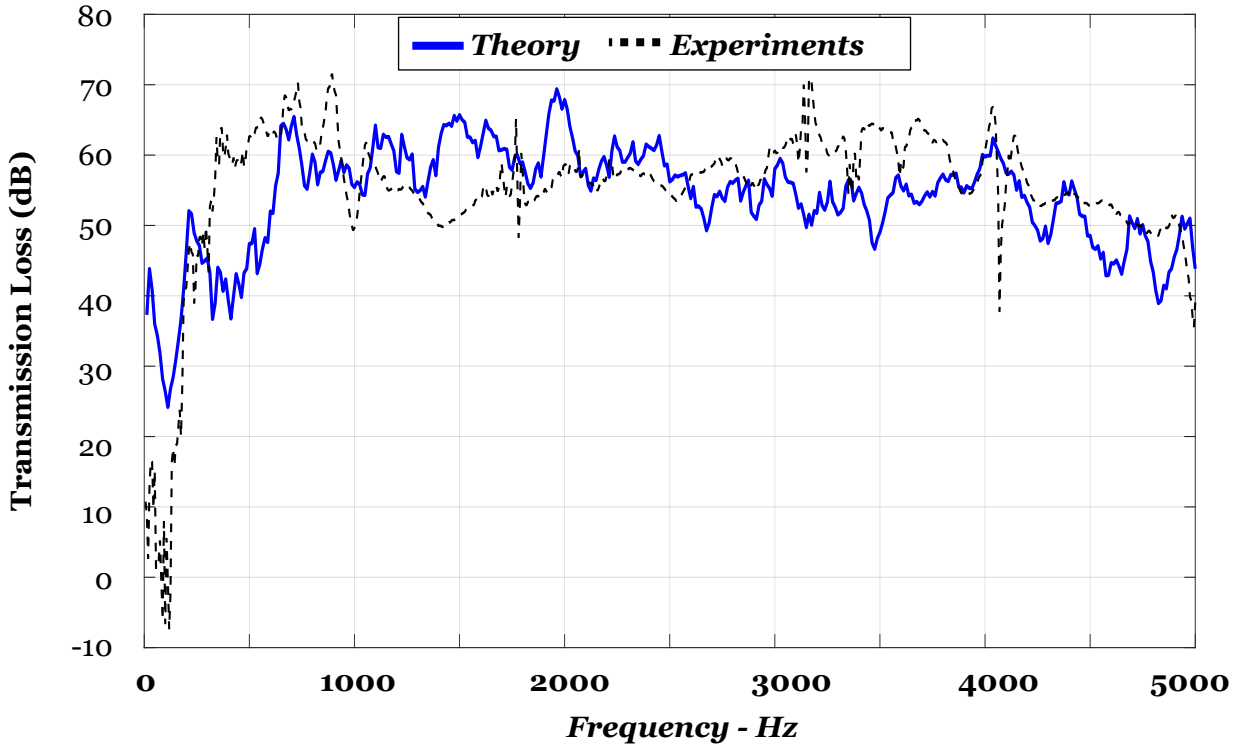

Figure 5.2: Comparison of theoretical and experimental performance of IAMM in positive condition

Above is the comparison of the performance of the IAMM in positive control scenario. The experimental performance of the IAMM exceeds the predicted model in the higher frequency range on 2500-5000 Hz. When pressurized IAMM exhibits resonance peaks around 1800 and 4100 Hz. The non-equivalency of the stress created in the membrane in both cases causes the performance to deviate from each other.

5.3 Negative control

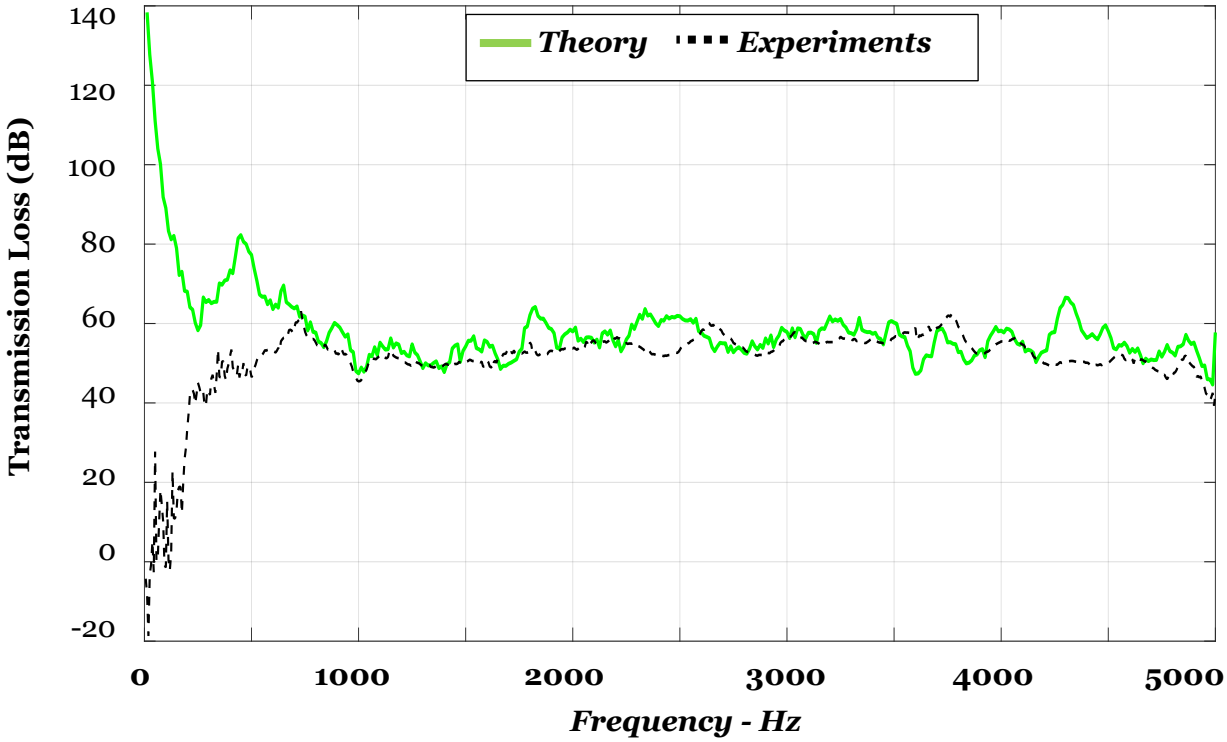

Figure 5.3: Comparison of theoretical and experimental performance of IAMM in negative condition

When vacuum is produced in the IAMM, the perforations shrink and thereby creating higher density in the sound pathway. The clear simulation of such scenario is hard to create as the absence of fluid transmissible substrate cannot be verified completely. Yet, it is very evident that the IAMM has better stable performance in this control scenario. The experimental performance of the IAMM in negative control exhibits a noise attenuation over a range of frequencies.

5.4 Summary

In this chapter the results from the Finite Element Analysis (FEA) is compared to the actual results from the experiments. The results from each control are compared individually. The chapter performs as a snapshot view to clearly understand the resultant performance of the IAMM.

Chapter 6: Conclusion and Future scope

6.1 Conclusion

The thesis is presented with comprehensive investigation, both theoretically and experimentally of the proposed IAMM. The novel MAMs utilizes non-linear deformation and change in its geometrical stiffness for acoustic noise attenuation. The required deformation is produced by inflating and deflating the acoustic meta-material using air pumps.

The proposed metamaterial is perforated in specific star shaped divots, that give it negative Poisson's ratio. Theoretical understanding of the phenomenon that this property enables by change in geometrical stiffness when inflated are presented. Advanced additive manufacturing techniques like Multi-jet manufacturing is used to fabricate the needed prototype of IAMM.

The IAMM is modelled using commercial CAD software and simulated in FEA package ANSYS. The theoretical performance predicted by the package is then validated experimentally using an impedance tube. ASTM procedures were followed to ratify the results. The obtained results show how the IAMM can be tuned and how its noise attenuation can be manipulated.

6.2 Recommendation for future studies

The work presented here explores the advent of novel Inflatable Acoustic Meta-Material. It is opportune to truly understand the relationship between pressure applied, which corresponds to the stress created in the membrane, and transmission loss characteristic. There exist multiple forays which can be adopted to understand the extent of application of such an acoustic treatment.

Other methods to create the same change in geometric stiffness should be explored. The expansion of data-set linking noise attenuation to actuation of the IAMM can facilitate machine learning algorithms to further optimize the performance. The natural next step in such an exploration of IAMM is to install it in a headset for actual real time applications.

Bibliography

[1] B. Banerjee, "*An Introduction to Metamaterials and Waves in Composites",* Taylor and Francis, 2011.

[2] History of metamaterials - Wikipedia, 2021. En.wikipedia.org,

[3] Z. Liu, "Locally Resonant Sonic Materials", *Science*, Vol. **289**, No. 5485, pp. 1734-1736, 2000.

[4] J.Pendry, A.Holden, W.Stewart, and I. Youngs, "Extremely Low Frequency Plasmons in Metallic Mesostructures"*, Physical Review Letters*. **76**, 4773-477, 1996.

[5] J.Pendry, A.Holden,D. Robbins, and W. Stewart, "Magnetism from conductors and enhanced nonlinear phenomenon*", IEEE Transactions on Microwave Theory and Techniques*, **47**,2075-2084,1999.

[6] D.Smith,W.Padilla, D.Vier,S. Nemat-Nasser and S.Schultz, Composite Medium with Simultaneously Negative Permeability and Permittivity, *Physical Review Letters*, **84**, 4184-4187, 2000.

[7] V.Veselago, "The electrodynamics of substances with simultaneously negative values of and" , *Soviet Physics Uspekhi*, **10**, 509-514, 1968.

[8] R.Shelby , "Experimental Verification of a Negative Index of Refraction", *Science*, **292**, 77-79, 2001.

[9] K.M. Ho, C.K. Cheng, Z. Yang, X.X. Zhang, P. Sheng, "Broadband locally resonant sonic shields", *Applied Physics Letters,* **83**, 5566–5568, 2003.

[10] Z. Yang, J. Mei, M. Yang, N.H. Chan, P. Sheng, "Membrane-type acoustic metamaterial with negative dynamic mass", *Physical Review Letters* **101** 204301, 2008.

[11] S.H. Lee, C.M. Park, Y.M. Seo, Z.G. Wang, C.K. Kim, "Acoustic metamaterialwith negative density", *Physics Letters A* **373**, 4464–4469, 2009.

[12] N. Sui, X. Yan, T.-Y. Huang, J. Xu, F.-G. Yuan, Y. Jing, "A lightweight yet sound-proof honeycomb acoustic metamaterial", *Applied Physics Letters* **106** 17190, 2015.

[13] S.H. Lee, C.M. Park, Y.M. Seo, Z.G. Wang, C.K. Kim, "Acoustic metamaterial with negative modulus", *Journal of Physics: Condensed Matter* **21** 175704, 2009.

[14] J. Fey, W.M. Robertson, "Compact acoustic bandgap material based on a sub-wavelength collection of detuned Helmholtz resonators", *Journal of Applied Physics*, **109** 114903, 2011.

[15] J. Li, C.T. Chan , "Double-negative acoustic metamaterial", *Physical Review* **E70**, 055602, 2004)

[16] S. Guenneau, A. Movchan, G. Pétursson, S.A., Ramakrishna "Acoustic metamaterials for sound focusing and confinement", *New Journal of Physics* **9**, 399, 2007.

[17] M. Yang, G. Ma, Z. Yang, P. Sheng , "Coupled membranes with doubly negative mass density and bulk modulus", *Physical Review Letters* **110** , 134301, 2013.

[18] B. Liang, B. Yuan, J.-C. Cheng , "Acoustic diode: rectification of acoustic energy flux in one-dimensional systems", *Physical Review Letters* **103** 104301, 2009)

[19] S. Zhang, C. Xia, N. Fang, "Broadband acoustic cloak for ultrasound waves", *Physical Review Letters* **106** 0243011, 2011.

[20] J.J. Park, C.M. Park, K.J.B. Lee, S.H. Lee, "Acoustic superlens using membrane-based metamaterials", *Applied Physics Letters* **106** 051901, 2015.

[21] Z. Yang, H.M. Dai, N.H. Chan, G.C. Ma, P. Sheng, "Acoustic metamaterial panels for sound attenuation in the 50–1000 Hz regime", *Applied Physics Letters* ,**96** , 041906, 2010.

[22] A. Baz, "The structure of an active acoustic metamaterial with tunable effective density", *New Journal of Physics* **11**, 123010, 2009.

[23] A. Baz, "An active acoustic metamaterial with tunable effective density", *Journal of Vibration and Acoustics,* **132**, 041011, 2010,

[23] W. Akl, A. Baz, "Multi-cell active acoustic metamaterial with programmable bulk modulus", *Journal of Intelligent Material Systems and Structures* **21**, 541–556, 2010.

[24] W. Akl, A. Baz, "Analysis and experimental demonstration of an active acoustic metamaterial cell", *Journal of Applied Physics* **111**, 044505, 2012.

[25] B.I. Popa, L. Zigoneanu, S.A. Cummer, "Tunable active acoustic metamaterials", *Physical Review B* **88**, 024303, 2013.

[26] X. Chen, X. Xu, S. Ai, H. Chen, Y. Pei, X. Zhou, "Active acoustic metamaterials with tunable effective mass density by gradient magnetic fields", *Applied Physics Letters* **105**, 0719131, 2014.

[27] F. Langfeldt, J. Riecken, W. Gleine, and von Estorff. "A membrane-type acoustic metamaterial with adjustable acoustic properties", *Journal of Sound and Vibration*, **373**, 1-18, 2016.

[28] F. Langfeldt, H. Kemsies,W. Gleine, and von Estorff. "Perforated membrane-type acoustic metamaterials", *Physics Letters A*, **381**, 1457-1462, 2017.

[29] M. Bianchi, and F. Scarpa, "Vibration transmissibility and damping behavior for auxetic and conventional foams under linear and nonlinear regimes", *Smart Materials and Structures,* **22**, 084010, 2013.

[30] L. Mizzi, E. Mahdi,K. Titov,R. Gatt, D. Attard,K. Evans, and J. Grima, et al., "Mechanical metamaterials with star-shaped pores exhibiting negative and zero Poisson's ratio", *Materials Design,* 2018.

[31] S. Cailleaux,N. Sanchez-Ballester,Y. Gueche,B. Bataille, and I. Soulairol," Fused Deposition Modeling (FDM), the new asset for the production of tailored medicines", *Journal of Controlled Release*, **330,** 821-841, 2021.

[32] J. Jakubiak, and J. Rabek, "Three-dimensional (3D) photopolymerization in the stereolithography *Part II* Technologies of the 3D photopolymerization", *Polimery*, **46**, 164-172, 2001.

[33] Connex3 Objet500 and Objet350 Multi-Material 3D Printers — Stratasys.

[34] C. Armstrong,N. Todd,A. Alsharhan,D. Bigio, and R. Sochol, “3D Printed Morphing Nozzle to Control Fiber Orientation during Composite Additive Manufacturing”, *Advanced Materials Technologies*, **6**, 2000829, 2021.

[35] MED610, MED620 MED625FLX : Biocompatible 3D Printing Materials — Stratasys, (2021). Stratasys, Available:https://www.stratasys.com/materials/search/biocompatible.

[36] K. Mulholland and H. Parbrook, “The measurement of transmission loss”, *Journal of Sound and Vibration*, **5**, 391-394, 1967.

[37] A. Whatmore and M. Lowson, “Simple sound transmission loss measurements using a modified impedance tube technique”, *Applied Acoustics*, **6**, 293- 300, 1973.

[38] Frequency sweeps: Anton Paar Wiki, Anton Paar, Available: https://wiki.anton-paar.com/en/frequency-sweeps/.

[39] B. Ang. “Tips on using Frequency Sweep and List with your Function Generator”— Keysight Blogs, Blogs.keysight.com, 2021.

[40] GRAS Sound and Vibration, 2021. Kemar.us.

[41] SR780 - Dynamic Signal Analyzer, 2021. Thinksrs.com,